Development of High Sensitivity Nanobiosensor for Detection of Biomarkers of Cardiovascular Disease

Mr. Weerachon Phoohinkong

Mr. Yutthana Phimthong-Ngam

Dr. Rattapong sungnoon

Et al.

Suan Dusit University

2558

Development of High Sensitivity Nanobiosensor for Detection of Biomarkers of Cardiovascular Disease

Mr. Weerachon Phoohinkong
Faculty of Science and Technology
Mr. Yutthana Phimthong-Ngam
Faculty of Science and Technology
Dr. Rattapong Sungnoon
Faculty of Medicine, Chiang Mai University
Et al.

Suan Dusit University
2558

(this research was supported in part by national budget for research, in the fiscal year 2556)

หัวข้อวิจัย	การพัฒนานาโนไบโอเซนเซอร์ความไวสูงสำหรับตรวจวัดสารบ่งชี้ทางชีวภาพของโรคหัวใจและหลอดเลือด	
ผู้ดำเนินการวิจัย	นายวีรชน	ภูหินกอง
	นายยุทธนา	พิมพ์ทองงาม
	นายแพทย์รัฐพงศ์	สังข์หนุน
	นางสาวหฤทัย	ขันเพชร
	นางสาวลัดดาวัลย์	แสโสดา
	นางสาวกัญญาณัติ	คงหนองลาน
ที่ปรึกษา	รศ.ดร.เกสร	สุวรรณประเสริฐ
หน่วยงาน	คณะวิทยาศาสตร์และเทคโนโลยี มหาวิทยาลัยสวนดุสิต	
ปี พ.ศ.	2558	

จุดมุ่งหมายของการวิจัยครั้งนี้เพื่อศึกษาคุณสมบัติของวัสดุที่ใช้ประกอบและวงจรตรวจวัดของเซนเซอร์ไฟฟ้าเคมีสำหรับตรวจวัดสารไนตริกออกไซด์ซึ่งเป็นสารบ่งชี้ทางชีวภาพของโรคหัวใจและหลอดเลือด โดยเริ่มต้นศึกษาในส่วนของการตรวจสอบการตอบสนองต่อไนตริกออกไซด์ของเซนเซอร์ที่ประดิษฐ์จากชั้นของเตตระ ซัลโฟเนต ฟทาโลไซยานีน(NiTsPc) และ พอลิอะมิโดเอมีน (PAMAM) ที่กระกอบบนขั้วไฟเบอร์คาร์บอน (CF) จากผลการทดลองพบว่าเซนเซอร์ที่มีโครงสร้างแบบ CF-(PAMAM/NiTsPc) มีประสิทธิภาพในการตรวจวัดสารไนตริกออกไซด์สูงกว่าเซนเซอร์ที่ปรับปรุงขั้วตรวจวัดรูปแบบอื่นๆโดยเซนเซอร์ชนิดนี้สามารถตรวจวัดไนตริกออกไซด์แม้มีสารรบกวนที่มีความเข้มข้นสูงที่ละลายในน้ำ เช่น ไนเตรตไอออน (NO_2 –), ไฮโดรเจนไดออกไซด์ (H_2O_2), โดพามีน (DA), กรดยูริค (UA), นอร์เอพิเนฟริน(NEp), อิพิเนฟริน (Ep) and กรดแอสคอร์บิค(AA) ความสัมพันธ์เชิงเส้นที่มีค่าสัมประสิทธิ์สหสัมพันธ์ (R) ที่ 0.9732 ในช่วงความเข้มข้น 8-80 µmol ของไนตริกออกไซด์ ค่าความไวของเซนเซอร์ที่พิจารณาจากความชันของเส้นถดถอยที่ 5.54 pA· µmol $^{-1}$ ขีดจำกัดของการตรวจจับของเซนเซอร์ที่พิจารณาความเข้มข้นที่สอดคล้องกับสัญญาณรบกวนในอัตราส่วน 3: 1 พบว่ามีค่าเท่ากับ 5.5 µmol

การศึกษาต่อมาเป็นการศึกษาความก้าวหน้าของเซนเซอร์ไฟฟ้าเคมีที่ปรับปรุงคุณสมบัติด้วยโลหะและสารเซมิคอนดักเตอร์พบว่าอนุภาคนาโนของทองที่ปรับปรุงขั้วไฟฟ้าอินเดียมทินออกไซด์ด้วยเทคโนโลยีชั้นต่อชั้นบน (3-เมอร์แคปโตโพร์พิลล์)-ไตรเมทอกซีไซเลน โซเจฟิล์มแสดงให้เห็นค่าความไวสูงและความจำเพาะที่ดีต่อไนตริกออกไซด์ ต่อมาเมื่อพิจารณาอนุภาคนาโนของ Pt–Fe (III) บนขั้วแกลสซีคาร์บอนมีขีดจำกัดการตรวจจับของเซนเซอร์ต่ำประมาณ 0.31 nmol • L-1 และมีช่วงการวัด

เป็นเชิงเส้นที่กว้าง (12 nmol • L^{-1} - 0.7mmol • L^{-1}) การศึกษาอนุภาคนาโนของ α-Fe2O3บนแกลสซีคาร์บอนพบว่ามีเวลาการตอบสนองที่ 5 วินาที และมีความเป็นเชิงเส้นในการตรวจวัดอยู่ในช่วง5.0×10^{-7} ถึง 15.0×10−6 mol· L^{-1}มีค่าขีดจำกัดการวัดอยู่ที่ 8.0×10−8 mol·L^{-1} และค่าความไวอยู่ที่ −283.6 μA/mmol·L^{-1}

การศึกษาขั้นสุดท้ายนำเสนอการออกแบบวงจรขยายที่มีสัญญาณรบกวนต่ำและใช้พลังงานต่ำ สำหรับการประยุกต์ใช้กับไบโอเซนเซอร์แบบบูรณาการการออกแบบประสบความสำเร็จในการออกแบบวงจรทรานส์อิมพีแดนซ์ 5MΩ ที่มีอัตราขยาย 981aA/√Hz @ 1kHz ของสัญญาณรบกวนขาเข้า พลังงานเท่ากับ 8.06μW ที่แหล่งจ่ายไฟ 0.9V

Research Title	Development of High Sensitivity Nanobiosensor for Detection of Biomarkers of Emerging Disease and Cardiovascular Disease	
Researcher	Mr. Weerachon	Phoohinkong
	Mr. Yutthana	Phimthong-Ngam
	Dr. Rattapong	Sungnoon
	Ms. Harutai	Khunphet
	Ms. Laddawan	Sangsoda
	Ms. Kanyanat	Kongnonglan
Research Consultants	Assoc.Prof.Dr. Kesorn	Suwanprasert
Organization	Faculty of Science and Technology Suan Dusit University	
Year	2015	

The aim of this work was to study a fully materials properties and measuring circuit of electrochemical sensor to detect nitric oxide which is a biomarkers of cardiovascular disease. The initial step in this study involved investigation of the response to NO of a sensor based on alternate nickel tetrasulfonated phthalocyanine (NiTsPc) and Polyamidoamine (PAMAM) layers assembled on a carbon fiber (CF) electrode was developed. The CF-(PAMAM/NiTsPc) sensor showed the best performance for NO detection when compared to another modified electrodes. For example, this sensor type is able to detect NO in aqueous solutions in the presence of high concentrations of interferents such as nitrite ion(NO_2^-), hydrogen peroxide (H_2O_2), Dopamine (DA), Uric acid (UA), norepinephrine (NEp), epinephrine (Ep) and Ascorbic acid (AA). A linear correlation with a correlation coefficient (R) of 0.9732 was obtained in the concentration range from 8 to 80 μmol of NO. The sensitivity of the sensor determined from the slope of the regression line was found to be 5.54 $pA \cdot \mu mol^{-1}$ The limit of detection of the sensor, determined as the concentration corresponding to a signal to noise ratio of 3:1 was found to be 5.5 μmol.

Later studies have mainly addressed recent advances of electrochemical NO sensors based on metal and semiconductor. Found that Gold nanoparticle (AuNPs) modified indium tin oxide (ITO) electrode by the layer-by-layer technology on a (3-

mercaptopropyl)-trimethoxysilane sol–gel film, which displays high sensitivity and excellent selectivity towards the determination of NO. The detection limit of the NO sensor is as low as 0.31 nmol·L−1, and the linear range is also wide (12 nmol·L−1 - 0.7mmol·L−1).an electrochemical sensor for sensing NO by electrodeposition of Pt–Fe (III) nanoparticle on a GC electrode. This sensor exhibits excellent electrocatalytic activity for the oxidation of NO. The linearity range of the sensor is between 8.4×10−8 and 7.8×10−4 mol·L−1 and the detection limit is 1.8×10−8 mol·L−1.Hematite (α-Fe2O3) nanoparticles were prepared by a simple solution-combusting method and dispersed in chitosan solution to fabricate nanocomposite film on GC electrode, that has response time of 5 s, linearity as 5.0×10−7 to 15.0×10−6 mol· L−1 of NO with a detection limit of 8.0×10−8 mol·L−1 and a sensitivity of −283.6 μA/mmol·L−1.

The final study proposes the design of a low-noise, low-power transimpedance amplifier for application in integrated electrochemical biosensor devices. The final proposed design achieves a 5MΩ transimpedance gain with 981aA/√ input inferred noise, 8.06μW at 0.9V power supply.

Acknowledgements

I would like to express my gratitude to all those who gave me the possibility to complete this research. I am deeply indebted to my advisor, Assoc. Prof. Dr. Kesorn Suwanprasert, whose help, suggestions, knowledge, experience and encouragement helped me in all the times of research and analysis of the research data in research period. In addition, special thanks for her guiding in a physiological background and giving me permission to commence this research in the first instance. I would like to thanks, research assessors, Asst. Prof. Dr. Jiraroj T.thenpracert for all advice and commendation.

I also would like to acknowledge a grant from under the National Research Council of Thailand. I wish to thank the Research and Development Institute of Suan Dusit University for all their Help, support, interest and valuable hints.

Finally, I would like to give my special thanks to elderly, physician, nurse public health officials and medical technician in the Northern Lower who have been provided data and well completion operations.

Researchers

2015

Contents

List of Tables

List of Figures

Chapter 1
Introduction

Background

Biosensor devices have found an increasingly broad range of applications, including but not limited to clinical, biological, environmental, and pharmaceutical testing and research. With ever increasing applications for biosensors, detection hardware in biosensors are required to cover an increasingly broad range of bio-signals. These signals often require very specifically designed detection hardware, to account for conditions such as very weak input signal coupled with high input noise.

The Biological markers or abbreviated as biomarker is a substance that our measurements of the human body to see if they are affected by chemical exposure in the environment or pathological conditions that can cause disease various.

Since nitric oxide (NO) was biologically identified as an endothelium-derived relaxing factor in 1987, there has been a great increase in the research of its chemistry, biology, and therapeutic actions. In 1992, NO was declared “molecule of the year” in Science. Since then, in addition to acting as the molecular messenger and vasodilator, NO has been found to be involved in a wide range of biological processes, including penile erection , neurotransmission, inhibition of platelet aggregation and immune response. In 1998, in recognition of their contribution to the field of NO research, three American scientists, Robert F. Furchgott, Louis J. Ignarro, and Ferid Murad, who first unraveled the complex nature of this simple molecule, were jointly awarded the Nobel Prize for Physiology or Medicine. Due to the importance of NO in biology, it is very important to accurately measure the concentration of NO in situ and in real time. However, its short half-life (~6 s) and high reactivity with biological compounds such as superoxide, oxygen, thiols and others, made the detection of NO very difficult. Many different techniques have been developed for the detection of NO in biological samples, including chemiluminescence, paramagnetic resonance spectrometry and imaging, and bioassay and electrochemical sensors. Among them, electrochemical sensors are of significance in NO detection because of its high sensitivity, good selectivity, fast response time, and long-term stability. In addition, these sensors are the only available

approach for in situ and real-time detection. In 1992, World Precision Instruments (WPI) made the first commercial electrochemical NO detection system, ISO-NO. Since then, they have continued to develop highly specialized and sensitive NO electrodes to detect the NO in a very small volume or single cell. In 2002, they successfully fabricated a nanometer-sized sensor with a tip diameter of just 100 nm. In addition to making extremely small NO electrochemical sensors, extensive efforts have been directed to improve the sensitivity and selectivity through electrode surface modification using nanomaterials. In this chapter, the nanostructure of the NO sensors will be addressed in the aseptic manner of nanometer-sized electrode and nanomaterials used for the modification of electrode.

Detection of nitric oxide (NO), one of the prominent representatives of reactive nitrogen species, is of high relevance but still represents a challenge in biomedical areas(Borgmann, 2009) . NO is involved in many physiological processes and can act not only as a regulatory but also as a pathological molecule. Since several pathologies have been associated with dysfunction in the endogenous production of NO, accurate quantification of NO levels and fluxes in different tissues is essential. There are several direct and indirect approaches available for NO detection ranging from bioassays to optical and electrochemical techniques. Electrochemical quantification of NO employing specifically designed NO sensors or its direct oxidation on different electrode materials is attractive because it enables direct quantification of NO both in vitro and in vivo.

Amperometric NO sensors are attractive because of their relative simplicity, fast response time and excellent sensitivity. However, their long-term stability for long-term monitoring of NO in tissues of living organisms remains a challenge. NO sensors owe their selectivity to the unique potential at whichNO is oxidized. However, several other species in the sample matrix, such as nitrite, nitrate and hydrogen peroxide may also be oxidized at similar potentials. Several approaches to improve the selectivity of NO sensors against potential interferents have been reported. For example, Nafion™ is commonly used as a selective membrane in NO sensing. This membrane reduces the impact of cationic interfering substances by electrostatic trapping, as well as acting as an impermeable membrane against negatively charged interferents.

Nitric oxide (NO) has recently emerged as a ubiquitous molecular mediator involved in a wide variety of biological processes in several organ systems (Tuteja, Chandra, Tuteja, & Misra, 2004). In brain, NO, or a related compound, appears to be a nonconventional neurotransmitter that may also participate in the regulation of the cerebral circulation (Riera, Schousboe, Waagepetersen, Howarth, & Hyder, 2008). NO is a diffusible, short-lived, and highly reactive chemical species that is difficult to measure in vivo (Kelm, 1999). Therefore, studies on the role of NO have most often utilized agents that inhibit the activity of NO synthase (NOS), the enzyme that synthesizes NO from L-arginine (Goldstein, Ostwald, & Roth, 1996). These agents, termed NOS inhibitors, are N"'-substituted L-arginine analogues that inhibit NOS competitively (Bratt, Zeki, Last, & Kenyon, 2011).

It is known that the NO radical is not only a physiological mediator but, if produced in excessive amounts, can be cytotoxic. Such cytotoxic properties are 'beneficial' in the sense that NO functions in immune-mediated reactions as a host defense mechanism against tumour cells and invading organisms (Pacher, Beckman, & Liaudet, 2007). In many cases, however, an overproduction of NO is thought to contribute to the development of disease states. For example, abnormally high concentrations of NO have been implicated in acute and chronic inflammation, in the systemic inflammatory response syndrome and in endotoxic shock (Uttara, Singh, Zamboni, & Mahajan, 2009). In such circumstances activation of peripheral blood monocytes, alveolar macrophages or neutrophils leads to expression of the inducible NO synthase, which synthesizes large amounts of NO. The NO then causes the enhanced vasodilatation and development of oedema which are characteristic of the inflammatory response. In endotoxic shock, increases in NO synthesis can be related to the degree of hypotension (Davies, Fulton, & Hagen, 1995). Nitric oxide-mediated vascular endothelial cell toxicity has also been described in vitro, in a study where endotoxin-induced loss of cell viability could be offset by dexamethasone, an inhibitor of the induction of NO synthase, or by the NO synthase inhibitor NG-monomethyl-Larginine (Palmer, Bridge, Foxwell & Moncada, 1992). NO owes its cytotoxic actions to its free radical nature. These actions include long-term inhibition of mitochondrial cytochrome oxidase, inactivation and degradation of aconitase and complex I and II of the mitochondrial electron transport chain, and inactivation of ribonucleotide reductase

with subsequent inhibition of DNA replication (Brown, 1995). In addition, NO has been shown to deplete cellular levels of glutathione (GSH) (Whit Walker, Kinter, Roberts, & Spitz, 1995). It may follow from this that total cellular GSH confers a significant proportion of the resistance of a cell to NO-mediated cytotoxicity. NO has also been shown to inactivate enzymes involved in the GSH redox cycle, such as GSH peroxidase (Asahi et al., 1995) and GSH reductase (Becker, Gui & Schirmer, 1995).Cytotoxic events associated with NO may also result from its interaction with other ROS, such as H_2O_2 or superoxide, to form singlet oxygen (Noronha-Dutra, Epperlein, & Woolf, 1993) or peroxynitrite (Beckman, Beckman, Chen, Marshall & Freeman, 1990), respectively. Peroxynitrite and its degradation products can cause injury via oxidation of protein sulfhydryl groups, nitrosation of several tyrosine molecules which regulate enzyme function and signal transduction, or via lipid peroxidation (Davies et al. 1995). More recently, however, evidence has emerged that peroxynitrite may mediate at least some of the physiological effects previously attributed to NO and that GSH is an important cellular target under these circumstances (Mayer, Schrammel, Klatt, Koesling & Schmidt, 1995). It is therefore

Research Objectives

1. To study on the evaluation process for biomarkers of nitric oxide in the cardiovascular system for use with the biosensor for cardiovascular disease.
2. To study the effects of nanostructure for nitric oxide determination.
3. To study and design sensing circuit of biomarkers for cardiovascular disease.

Scope of Research

This work focuses on to design a biosensor prototype and prove its functionality by performing electrochemical detection of biomarkers (nitric oxide) for use in applications include measurement of biological indicators in cardiovascular disease.

Limitation

Research areas (Collect data and test samples) have ranged far and wide in rural areas (Northern Region), which takes a long time and high travel budgets.

Research Hypothesis

1. Nitric oxide is a highly effective biomarkers to evaluate patients with cardiovascular disease.
2. Nonmaterial can be improved performance of nitric oxide electrochemical sensors.
3. Transimpedance amplifier circuit can be applied to developed for the detection of nitric oxide in biological samples

Definitions of Research Terms

Accuracy: the closeness of a measured value to the known "true" value of the measurand.

Actuator: a device, which uses the signal, form the sensors to perform some action. An example can be an alarm with a smoke detector or a hydraulic valve coupled to a pH electrode.

Activity: the effective amount of a free ion in solution. The amount and type of other ions in the solution influence the chemical effectiveness of an ion, so that varying the solution composition makes a fixed concentration of a given ion more or less "active". In dilute solutions, ionic activity and concentration are practically identical, but in solutions containing many ions, activity may differ from concentration. Ionic activity, not concentration, determines both the rate and the extent of chemical reactions.

Activity coefficient: a factor, which relates the activity to the concentration of a species in solution, such that: Ax = FxCx (where: Ax = Activity of the species x; F_x = Activity coefficient of the species x; Cx = Concentration of the species x). The activity coefficient is dependent on the ionic strength of the solution (ions of similar size and charge have similar activity coefficients). It becomes progressively lower as

the ionic strength increases, due to inter-ionic interactions. The activity coefficient for any ion in solution can be calculated using the Debye-Huckel equation.

Analog multiplexer: a device that increases the number of measurements channels while still using a single instrumentation amplifier.

Asymmetry potential: the potential across a glass pH electrode membrane when the inside and outside of the membrane are in contact with solutions of identical pH. This term has also been used to define the observed potential differences between identical electrode pairs placed in identical solutions. Differences can occur because of variability in the potentials of the internal reference elements of both the sensing and the reference electrodes, differences in liquid junction potentials, and differences in internal filling solutions. These variations in electrode potential are compensated for by the instrument calibration control (asymmetry potential control).

AU: arbitrary unit.

Average number: the number of instantaneous readings of the sensor (e.g. electrode potential), taken for example at one-second intervals, used to calculate the average value for the millivolts. An operator-selectable variable in computer interface software which helps to reduce noise and increase the precision of ISE measurements.

Biosensing: Technology for the detection of a wide range of chemical and biological agents, including bacteria, viruses and toxins, in the environment and humans.

Biosensor: An electronic device that uses biological molecules to detect low levels of substances like proteins in the body or pollutants in water.

Calibration: a process of normalizing sensor output by measuring a series of two or more known concentration solutions. The ion analyzer then calculates the offset and slope characteristics of the electrode and uses them to compute the concentration of unknown samples.

Calibration curve: a plot of electrode potential versus activity in two or more standardizing solutions. Unknown sample activity is determined by converting electrode potential to activity using the curve.

Channel: a pin or wire lead to which we apply or form which we read the analog or digital signal.

Chemical sensor: a miniaturized analytical device, which can deliver real-time and on-line information on the presence of specific compounds or ions in the complex samples.

Chemooptical interface: the receptor part (see optomembrane) of a fiber optic chemical sensor containing an immobilized reagent (e.g. indicator, dye or chromoionophore), which converts chemical information on the sample into changes of its spectral properties (absorbance, fluorescence).

Combination electrode: a combination of a sensing electrode and a reference electrode contained in one unit.

Complexing agent: any species that combines with an ion to form an undissociated species; the resulting complex stays in solution and does not precipitate. Complexing agents are used as titrants and to bind ions that may interfere with direct measurements.

Concentration: the total mass of an ion or molecule in a given volume of solution (see: activity). When measuring ionic concentration by ion-selective electrodes, it is important to note that the concentration used in the calibration graphs and calculated for the samples is the concentration of the free ion in solution, not the concentration of the compound from which this ion is derived. A distinction must also be made between the concentration of the free unbound ions and the total concentration, which may include any ions, bound to complexing agents and any atoms in undissociated molecules.

Conductivity: a measure of the ability of a solution to conduct electricity. It is the reciprocal of resistivity, which relates the resistance of a conductor (in ohms), to its length and cross sectional area. Units of conductivity are Siemens per centimeter (S/cm). Conductivity is measured with a conductivity cell. This contains two platinum electrodes of known area rigidly fixed at 1 cm apart. The electrolytic conductivity of the solution is determined by passing an alternating current between the electrodes. The conductivity is related to the ionic strength of the solution.

Data acquisition (DAQ): process of acquiring data, typically from A/D or digital input plug-in devices.

Detection limit: the concentration at which the mean value of the output sensor signal is equal to two standard deviations. In practice, the lowest concentration of the

analyte that can be detected and/or measured by a sensor. In other words, the concentration (or activity) of the measured ion at the point of intersection between the extrapolated linear segment of the calibration curve (representing the normal slope of the electrode) and a horizontal line (representing the voltage when the concentration is so low, that small changes in concentration do not produce any detectable change in the electrode response). The portion of the calibration curve between this point and the beginning of the truly linear section is known as the non-linear range of the electrode. Samples are still measurable within this range provided that several standards are used to define the changing slope of the curve accurately, but the error in concentration (per millivolt error in measurement) will be progressively greater as the slope reduces.

Detector: a device, which indicates the presence of the chemical species above a predetermined, threshold value. There is not explicit qualitative relationship between the output and stimulant.

Direct potentiometry: the simplest method of making ion-selective electrode measurements. The electrodes are immersed in a test solution and the electrode potential is measured directly with a millivolt meter. The concentration is then related directly to this measurement by reading the answer from a calibration graph of concentration versus milivolts.

Dynamic range: the range of concentrations in which the sensor sensitivity is greater than zero. The dynamic range can be also expressed as the difference between minimum and maximum signal values of the sensor in steady-states.

Error (of a measurement): the result of a measurement minus a true value of the measurand.

Interface: an electronic device, which allows connecting the output from a sensor directly to a desk-top or lap-top computer without the need for an expensive ion meter. Interfaces are provided with sophisticated software, which facilitates complex data processing, display and storage. Multiple interfaces can connect several electrode systems to one PC at the same time and permit continuous monitoring of batch processes or simultaneous multi-component analysis.

Linear range: the range of concentration (or activity) over which the measured sensor signal can be fitted by straight line.

Measurand: particular quantity subject to measurement.

Measurement: set of operations having the object of determining the value of a quantity.

Noise: abrupt, random, small changes in displayed sensor signal (in electrode, usually due to the pickup of strong static charges). Noise may be caused by air bubbles, poor conductors, or high electrical resistance somewhere in the circuit.

Open circuit: lack of electrical contact in any part of the measuring circuit (which consists of the sensing electrode, instrument, reference electrode and solutions). An open circuit is characterized by rapid large jumps in displayed potential, followed by an off-scale reading. Frequent large erratic changes in potential indicate an intermittent open circuit.

Random error: a result of a measurement minus the mean that would result from an infinite number of measurements of the same measurand carried out under repeatability conditions.

Receptor part: according to the IUPAC definition of chemical sensor one of the two principal components of the chemical sensor, which converts chemical information into a form of energy.

Reference electrode: the half of an electrode pair which provides a constant potential, regardless of the sample composition. The potential developed by a sensing electrode is measured against this reference to give a signal, which can be converted to the activity of ion under analysis. Single junction reference electrodes have a single chamber generally filled with a potassium chloride solution saturated with silver chloride, which contacts with the sample solution through a single liquid junction by means of a semi-porous ceramic plug or fritted disc. Double junction reference electrodes have two chambers with the internal reference system having a liquid junction with an intermediary salt bridge and then a second liquid junction to the external sample. The outer filling solution is chosen to avoid contamination of the sample and minimize the effects of the liquid junction potential.

Reproducibility: the closeness of replicate measurements on the same sample, using the same measuring technique, under the same conditions. Reproducibility can be limited by many factors, including instrument or electrode stability, loss of the substance being measured during sample operation and contamination.

Response time : the length of time necessary to obtain a stable electrode potential when the electrode is removed from one solution and placed into another of different concentration or temperature. Response time depends on the electrode type, the measuring solution, the magnitude and direction of the concentration change, temperature, and the presence of electrode, if any. The response time can be expressed as the time at which the output reaches 63% (1/e) or 95% of its final value, in response to a step changes in concentration.

Result of measurement: a value attributed to a measurand, obtained by measurement.

Selectivity: the ability of the device to measure one chemical component in the presence of others in the sample. For example ion-selective electrodes are not 100% ion-specific. Most are sensitive to some other ions to some extent. Some ISEs cannot be used in the presence of certain other interfering ions or can only tolerate very low contributions from these ions. Special techniques are available for removing or compensating for interfering ions.

Sensitivity: the slope of the response (calibration) curve expressed as output per unit concentration.

Sensor: a device for transducing information about the concentration of a chemical species into a readily accessible signal (usually electrical). The device responds directly to the amount of a given environmental component. Ion selective electrodes are sensors, which respond to the concentration of particular dissolved ions in a solution.

Sensor array: a set of sensors with different sensitivity and limited selectivity. Sensors array provide multiple data points per sample (vector of data) that carry out additional chemical information to differentiate analytes and discriminates against interferences. The pattern of response (distinct for different compounds) of an array of sensors can be applied to identify the unknown component. Suitable pattern-recognition algorithms are used to interpret the results of multielement arrays.

Stability: the percent of change of the baseline and/or sensitivity in time.

Systematic error: mean that would result from an infinite number of measurements of the same measurand carried out under repeatability conditions minus a true value of the measurand.

Transducer: a physical part of the sensor (detector), which amplifies the primary signal to usable level. According to the IUPAC definition of chemical sensor one of the two principal components of the chemical sensor. The receptor part converts chemical information into a form of energy acceptable by the transducer and then the analytical signal is generated.

Uncertainty (of a measurement): parameter associated with the results of a measurement, which characterizes the dispersion of the values that could reasonably be attributed to the measurand.

Projected Benefits of the Research

1. A new approach to evaluation process for biomarkers of nitric oxide in the cardiovascular system for use with the biosensor for cardiovascular disease.
2. Know about the effects of nanostructure for nitric oxide determination.
3. A new approach to high efficiency biosensor circuit design of biomarkers for cardiovascular disease.
4. Findings can be published in a national or international journals have at least one issue and can be applied to hospitals or health centers in rural areas more effectively.

Chapter 2
Theory and Related Research

Nitric Oxide Biomarker

Nitric Oxide (NO) is formed from the guanidine-nitrogen terminal of L-arginine by the enzyme NO synthase (NOS), which has 3 major isoforms: eNOS found in endothelial cells, nNOS found in NO producing neurons, and cytokine-inducible iNOS. A mitochondrial enzyme (mtNOS) may also exist (Tengan, Rodrigues, & Godinho, 2012) although there is controversy as to whether it is a true NOS isoform. These isoforms differ in function, amino acid sequence, post-translational modification, and cellular location. O_2 is required for enzymatic synthesis of NO from L-arginine, therefore O_2 availability affects NO production rates for all three major NOS isoforms. Once NOS is maximally activated, the rate of NO generation depends primarily upon available concentrations of L-arginine and O_2.

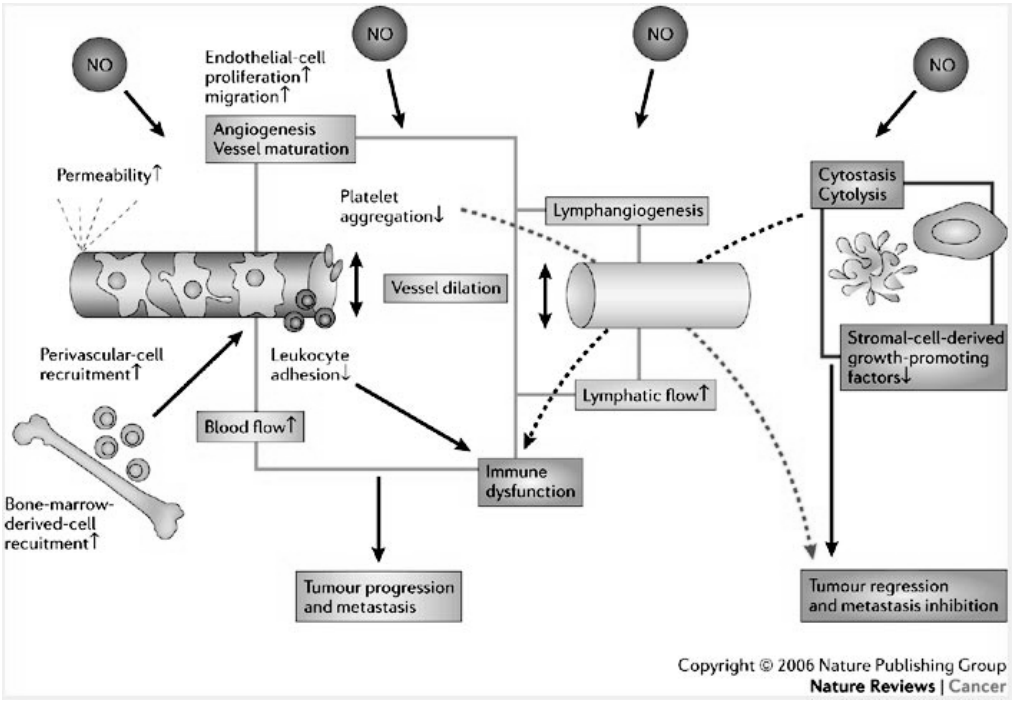

Figure 2.1 Mechanisms of action of NO

Activation of constitutive NOS (eNOS and nNOS) depends upon intracellular Ca^{2+} and calmodulin (Kuchan & Frangos, 1994), although some studies suggest there may also be a Ca^{2+}-independent pathway. Increased Ca^{2+} promotes binding of Ca^{2+}-calmodulin to eNOS and nNOS, displacing caveolin to produce NO (Russell et al., 2000). Increases in Ca^{2+} can be stimulated by acute increases in shear stress or by activation of G-protein coupled cell surface receptors. Therefore NO release can be modulated by changes in shear stress exerted on the arterial wall by flowing blood or by agonists in the bloodstream. Fluid shear stress due to blood flowing through a vessel exerts a force on the luminal surface of the endothelium. Under basal conditions, the endothelial cytoskeleton is maintained under tension. When an external stimulus is applied, intracellular tension is redistributed over the cytoskeletal network. This architecture permits forces to be directly transmitted from the cell surface, through the cytoskeleton, and across physically interconnecting filaments to the nucleus (Chiu & Chien, 2011). These changes in force lead to the activation of eNOS through mechano or mechano-chemical signaling processes (Hsiao & Tsai, 2008). Factors affecting the blood velocity, including fluid viscosity and the physical dimensions of blood vessels determine the shear stress action on the endothelium. Mean (time-averaged) shear stress tends to be highest in small arterioles (60-80 dynes/cm^2) and has been shown to cause a steady NO response during stimulation and a biphasic rise in Ca^{2+} concentration. Neurohumoral mediators (e.g. acetylcholine), circulating hormones (catecholamines and vasopressin), autoacoids generated within the vascular wall (bradykinin and histamine), or mediators released by platelets (serotonin, ADP) or formed during coagulation (thrombin) can also cause the release of NO through activation of specific endothelial receptors The inducible isoform (iNOS) does not require Ca^{2+} for activation. It can be induced in tissue by macrophages in response to endotoxins or cytokines. Excessive NO production has been implicated in inflammation and septic shock.

Constitutive NOS isoforms have been shown to play an important role in control of vascular tone (Chen, Pittman, & Popel, 2008). After formation, NO diffuses to vascular smooth muscle cells and stimulates soluble guanylate cyclase (sGC), resulting in increased cyclic 3’5’-guanosine monophosphate (cGMP) and vasodilation. This process catalyzes the conversion of guanosine triphosphate to cGMP and leads to the relaxation of smooth muscle cells (Denninger & Marletta, 1999). Some studies have

found evidence that, in the absence of eNOS, other vasodilator pathways compensate to preserve vascular tone. In eNOS-deficient (genetic knockout) mice, nNOS has been suggested as a mechanism by which vasodilation is maintained in the coronary circulation (Durand & Gutterman, 2013). In atherosclerotic vessels, increased nNOS expression was found to be associated with decreased expression or activity of eNOS, suggesting a possible compensatory mechanism (Levy, Chung, Kroetsch, & Rush, 2009).

Nitric Oxide Synthases

The NOS enzymes are polypeptides containing an N-terminal oxygenase domain and a C-terminal reductase domain. The molecular weights of these proteins have been shown to range from 140 – 150 kDa for nNOS and eNOS and are ~200 kDa for iNOS (Tripathi & Krishna, 2008). Between the two domains is an approximate 30-amino acid recognition sequence for calmodulin. The oxygenase domains of the different NOSs contains a core region that binds heme, tetrahydrobiopterin, L-Arginine, and forms the active site where NO synthesis takes place (Stuehr, 1999). The N-terminal region of the oxygenase domain is located upstream from the core region and varies in length between the different NOS isoforms. The N-terminal region participates in cellular targeting and may affect NOS structure or catalysis (Stuehr, 1999). The reductase domains of the NOS isoforms bind flavin mononucleotide, flavin adenine dinucleotide, and NADPH (Stuehr, 1999). During NO synthesis, the reductase flavins obtain electrons from NADPH. These electrons are then transferred to the heme iron, which permits it to bind and activate O_2 and catalyze NO synthesis. In the constitutive NOS isoforms, the flavin to heme electron transfer is triggered by calmodulin binding. The flavin to heme electron transfer is proposed as the mechanism by which calcium and calmodulin regulate NO synthesis from these isoforms. Certain proteins have been shown to inhibit or induce constitutive NOS activity, such as caveolin or heat shock proteins (e.g. Hsp90), although the mechanisms are not yet well understood (Stuehr, 1999).

NO production has been shown to be dependent on extracellular L-arginine concentrations. Circulating L-arginine concentrations range from 50 – 200 μM, however levels within endothelial cells can reach concentrations of 800 μM or higher

(Pezzuto & Bohlen, 2008). The affinity of purified eNOS for L-arginine is in the low μM range ($K_m < 5$ μM), suggesting that the enzyme operates under saturating substrate concentrations and should not respond to changes in extracellular L-arginine concentrations (Schmidt, Kolesnik, Gorren, Werner, & Mayer, 2014). However, studies have also shown that L-arginine supplements enhance endothelial-dependent vasoactivity (Böger et al., 2007). The dependence of eNOS on extracellular L-arginine despite saturating intracellular levels of L-arginine is known as the 'arginine paradox'. Hardy and May (2002) suggest that the paradox can be explained by regulated L-arginine uptake into a compartment that contains eNOS and that is distinct from bulk cytosolic L-arginine. The compartment may be associated with the caveolae (Hardy & May, 2002). However, future experimental work is needed to determine if such a compartment.exists and its precise location.

Under steady state, NOS circulates in an active cycle that generates NO and an inactive cycle that involves formation and decay of the heme-NO complex (Stuehr, 1999). NOS molecules start in a NO-free form during the active cycle, however once NO formation occurs, NO can bind to the enzyme molecules shifting the molecule to the inactive cycle. Decay of the NO complex enables NOS to become active once again, thus the enzyme can circulate in and between inactive and active cycles (Stuehr, 1999).

NO Synthesis

Oxygen is required for the synthesis of NO from L-arginine. The general oxidation reaction that occurs during a NOS active cycle to synthesize NO is

$$L - Arginine + O_2 \rightarrow L - citrulline + NO \qquad (2.1)$$

The generally accepted theory for how this process occurs is that heme reduction leads to O_2 binding and a stepwise activation of heme-bound O_2. Activation of the heme-bound O_2 generates the oxidant species that participate in NO synthesis (Stuehr, 1999). Experimental evidence suggests that distinct iron-oxygen species are involved in each step of NO synthesis although the precise mechanisms and distinct species are not well

characterized (Sato, Sagami, Daff, & Shimizu, 1998). NO production in the above reaction can be assumed to follow Michaelis-Menten kinetics, thus O_2 dependent NO production can be represented by

$$R_{NO} = \frac{R_{NO_{max}} C_{O_2}}{C_{O_2} + K_m}$$

where K_m is the Michaelis constant corresponding to the O_2 concentration (C)at half of the maximum NO production rate (R_{NOmax}) and R_{Nomax} is the maximum NO production rate (Buerk, 2001).

NO Reactions

NO reacts readily with oxygen and oxygen-derived radicals. The reaction between NO and O_2 to form nitrite (NO_2^-) is known as autooxidation. The oxidation reaction between NO and O_2 forms NO_2, which then decomposes to NO_2^- by the following set of reactions

$$2NO + O_2 \rightarrow 2NO_2$$

$$NO + NO_2 \rightarrow N_2O_3$$

$$N_2O_3 + H_2O \rightarrow 2NO_2^- + 2H^+$$

The kinetics of this reaction are second order in NO and first order in O_2 in aqueous environments such that

$$\frac{dC_{NO}}{dt} = kC_{NO}{}^2 C_{o_2}$$

where k is a general reaction rate constant, C_{NO} is NO concentration, C_{O2} and is O_2 concentration. This reaction occurs in the bloodstream, vascular wall, and tissue in microvessels, however, published rate constants for this reaction suggest that auto-oxidation has only minor influences on NO diffusion compared to other factors, such as reactions with hemoglobin or sGC, and may be neglected in most cases (Buerk, 2001).

Endothelial Dysfunction and Impaired Endothelial

Endothelial dysfunction and impaired endothelial derived NO bioactivity are associated with numerous disease states (Kolluru, Bir, & Kevil, 2012). Two common diseases associated with endothelial dysfunction are hypertension and atherosclerosis. Numerous studies have confirmed the importance of NO on the regulation of blood pressure during hypertension. In some models of hypertension, vascular NO is upregulated as a compensatory mechanism to attempt to return blood pressure to normal. In other cases, NO activity is decreased, leading to direct increases in systolic blood pressure (Loscalzo, 2000). The mechanisms thought to contribute to decrease NO bioactivity include decreased NOS levels, decreased sGC activity, and increased NO degradation. Established atherosclerosis or the presences of risk factors, such as hypertension or hypercholesterolemia, lead to dysfunctions in eNOS signaling (Stuehr, 1999). Proposed mechanisms that may contribute to atherosclerosis include decreases in NO production, increases in NO inactivation, and decreases in sensitivity to NO (Loscalzo, 2000). Other disease states associated with endothelial dysfunction include hypercholesterolemia, diabetes mellitus, congestive heart failure, ischemia/reperfusion, pulmonary hypertension, and vascular injury (Loscalzo, 2000). In this study, simulations were performed to simulate excessive production of superoxide, a factor associated with hypertension and atherosclerosis. There is currently a great deal of research to help elucidate the mechanisms of impaired endothelial function and associated NO bioactivity. Defects have been proposed to occur in all phases of the pathway leading from NOS3 gene expression to the actions of NO on the vascular system (Loscalzo, 2000). The general process involved in eNOS gene expression to endothelium-derived NO actions. Defects that can occur in this pathway are NOS3 poymorphisms, altered NOS3 expression and mRNA stability, impaired signal transduction between mRNA and eNOS, impaired eNOS substrate and cofactor availability, destruction of NO, and decreased responsiveness to NO. Two of these defects, impaired eNOS substrate availability and destruction of NO are modeled in this study. Understanding the mechanisms of “normal” NO bioactivity and transport can help further the understanding of impaired NO activity and its contribution to numerous disease states and lead to development of clinical therapeutics to treat these conditions.

Transimpedance Amplifier Circuit

Transimpedance amplifiers are used in a variety of applications, and cover an extremely broad range of specifications. Common applications include detecting signal from photodiodes in high-speed optical communication, and detecting current from accelerometers in micro electromechanical systems applications.

A transimpedance amplifier can be thought of simply as a current to voltage converter, which linearly converts a current input to a corresponding voltage output. The input/output relationship can be described using Ohm's law, and the overall transimpedance gain is measured in Volts/Amperes, or simply in Ohms.

Resistive Transimpedance Amplifier

A basic transimpedance amplifier can be constructed using an operational amplifier, a resistor, and a capacitor.

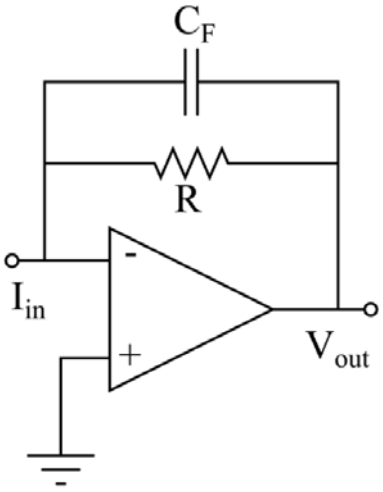

Figure 2.2 Basic resistive TIA circuit

Although simple, this design has several disadvantages. The primary disadvantage in this design is the need of a large resistor, which increases with the required transimpedance gain.

Continuous Time Transimpedance Amplifier

One method of avoiding the large resistor needed for high gain and high sensitive TIA design is the use of a resistor T-network to generate a large effective feedback resistance with smaller physical resistors. This topology can be used to achieve both a high transimpedance gain and low noise, while maintaining a large signal to noise dynamic range (Sharma, Zaman, & Ayazi, 2007).

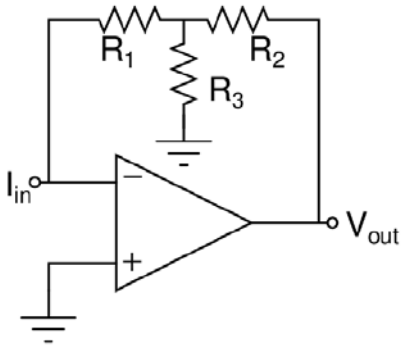

Figure 2.3 Showing T-Network TIA Schematic

Although this topology requires significantly less total resistance on chip than its equivalent single-resistor counterpart, the overall size reduction is often still not at the level required by designs of highly integrated biosensor arrays. An alternative TIA implementation employs the use of an active current reducing circuit in place of the resistor (Ferrari, Gozzini, & Sampietro, 2006).

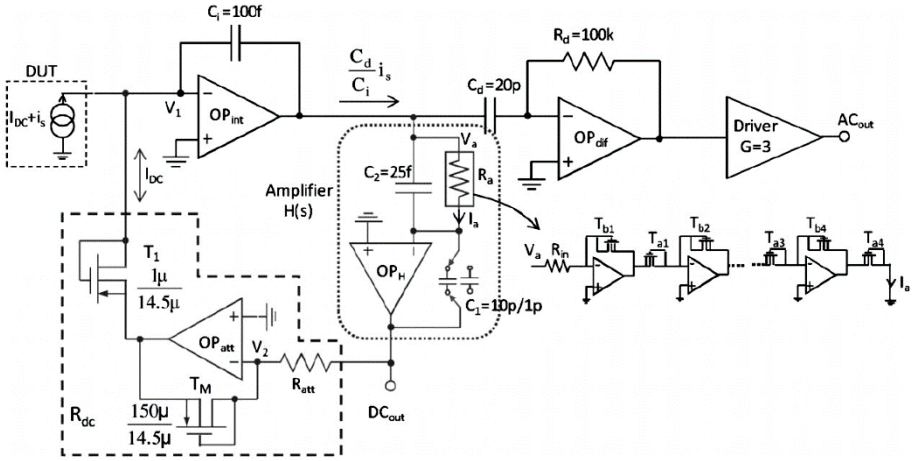

Figure 2.4 TIA with Active Feedback Network

This type of design can be used to emulate very high equivalent resistances of hundreds of GΩ with relatively high linearity. This design implements the current reducing circuit using a series of operational amplifiers which can increase power consumption while still maintaining a reasonable die area. This increased level of power consumption may not be suitable due to the stringent operating temperature requirements of live tissue on our biosensor applications. This design does manage to achieve an extremely low input noise level. Two other continuous time implementations involve using an active load and ratio of capacitors to generate high effective transimpedance gains. These designs tend to rely on extremely high impedance input biasing circuits, which can consume large amounts of die area. Despite this fact, this topology does tend to produce respectable input noise specifications (Bottino, Massobrio, Martinoia, Pruzzo, & Valle, 2009).

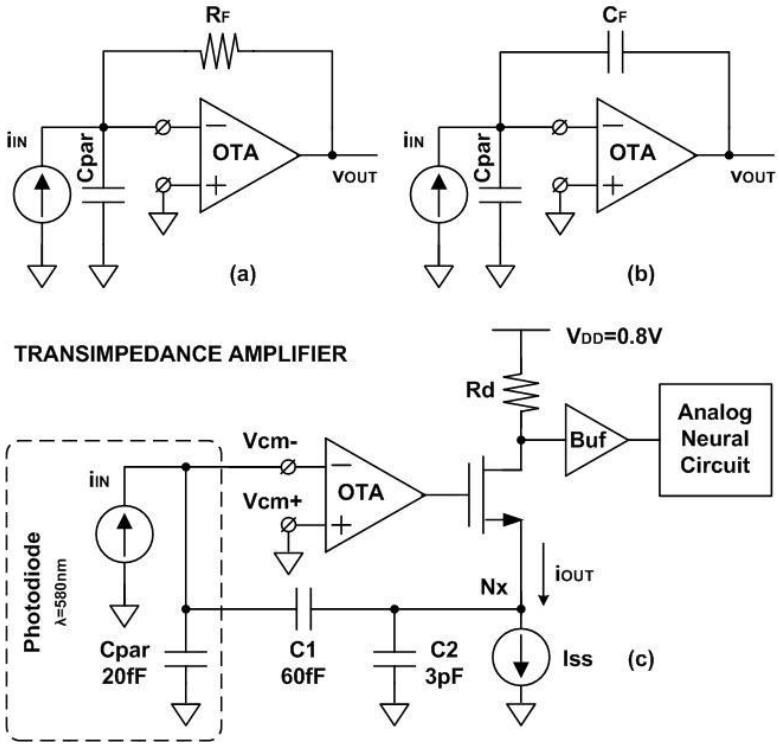

Figure 2.5 (a) Resistive feedback TIA; (b) Capacitive feedback TIA; (c) The schematic of the proposed TIA design with the improved capacitive feedback single-ended topology

An additional continuous TIA design intended for high-speed communication uses a simple resistive TIA topology with an added DC cancellation feedback network

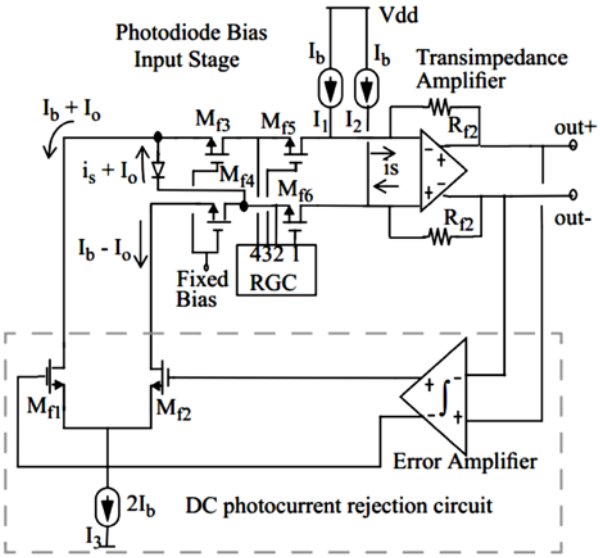

Figure 2.6 DC Cancelling TIA Schematic

The design achieves a bandwidth over 200MHz, and has a power consumption of 12mW at 3V. This significantly increased power consumption is needed for high bandwidth in optical communications. The DC cancellation feedback network is advantageous in communication, eliminating issues due to amplifier offset and 1/f noise. However, in a bio-signal application this DC cancellation can be problematic, causing a loss of slow-changing signals. A final continuous time implementation utilizes a unique configuration, consisting of a common-gate amplifier in parallel with a common-source amplification stage (Zand, Phang, & Johns, 2001).

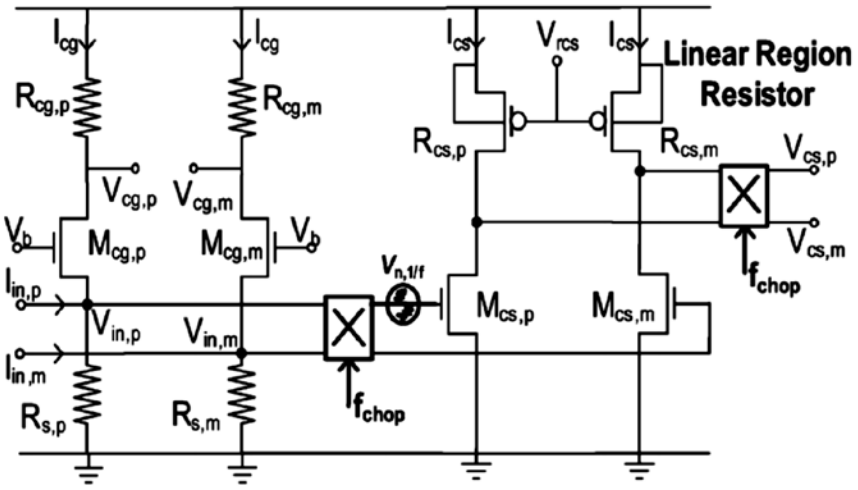

Figure 2.7 TIA common-gate/common-source Design

This combination of amplifier types and a chopper-stabilization technique are carefully used to reject 1/f noise. The overall circuit architecture shows promising results, achieving a low input-referred noise, as well as high overall linearity. Although this circuit performs well, the overall bandwidth and power consumption are significantly higher than our goal, and the overall circuit is likely to be larger than our application would allow (Balasubramanian et al., 2013).

Switched-Capacitor TIA Designs

Since large resistors (several to tens of MΩ's) can consume large amounts of die area and can be inaccurate once fabricated, an alternative is to replace the resistor with a "switched capacitor." This can be useful in larger scale voltage amplifiers, as well as transimpedance amplifiers. Switched capacitor implementations are also referred to as charge integrating transimpedance amplifiers. Special considerations such as charge injection and switch noise minimization or cancellation must be taken into account when using switching circuits with high sensitivity current measurements. Although switching can have undesirable effects in high sensitivity transimpedance amplifiers, it can be used to the designer's advantage, providing a means to effectively cancel undesired 1/f noise and amplifier offset through correlated double sampling. One such design uses a slow integrator, integrating the input current onto a capacitor and sampling the output voltage periodically. Integrator designs eliminate the need for a

large capacitor, and allow for low noise performance. This type of design has achieved spot noise specifications as low as 25fA/√Hz (Tang, Zhang, Fedder, & Carley, 2012).

A reduced noise floor is one of the main advantages of low-speed switched integrator designs. Allowing the signal to integrate over an extended period of time produces a reduction in switching noise and charge injection, leading to the potential for a lower overall input inferred noise current.

Biosensing Methods

Sensing methods currently in use include fluorescence spectroscopy, bioluminescence and chemiluminescence detection, and electrochemical detection. Fluorescence spectroscopy is a process of adding and tracking fluorescent light-responsive dyes or “label” molecules in a sample. Bio and chemiluminescence detection rely on the detection of a naturally luminescent substance in an analyte. Electrochemical detection uses a reduction or oxidation reaction (i.e. a redox process) to detect an electrochemically active analyte.

Fluorescence Detection

Fluorescence imaging detection involves adding a fluorescent label to the sample material. A filtered light source is used to create a single frequency excitation light. Application of the excitation light on a sample containing a fluorescent label causes photon emission from the fluorescent tag to occur at a different frequency, allowing for the optical detection of the fluorescent tag, its target, and their location. Typical fluorescence detection systems use either a high-performance single pixel detector with a scanning excitation source or a two-dimensional array of detectors, such as a CCD sensor, with a homogeneous excitation light source. In a fluorescence detection system, possible array size is determined by CCD implementation and the number of photosensitive pixels. In optical based systems; however, lenses and strategic illumination patterns can be utilized to achieve single-molecule measurement resolutions without the need to greatly reduce the scale of the detection devices.

\

Bioluminescence

Bioluminescence rely on the emission of light from the analyte. Although generally (but not necessarily) in the visible light spectrum, the small amount of light emitted is usually not visible to the human eye. Detection has been typically achieved with an extremely sensitive CCD sensor and photomultiplier tubes. CMOS image sensors have not been utilized in bioluminescence until more recently due to poor but improving performance and lower SNR.

Electrochemical Detection

Using a redox (reduction-oxidation) process, electrochemical detection can be used in a wide range of measurements under the condition that the analyte being measured is electrochemically active. Typical measurement instrumentation includes a two or three electrode system, where a potentiostat is used to hold a specific potential across a sample. Setting a specific potential between the reference (RE) and the working electrode (WE) can be used to selectively detect a specific analyte. The potentiostat also sources or sinks the required current through the counter electrode (CE).

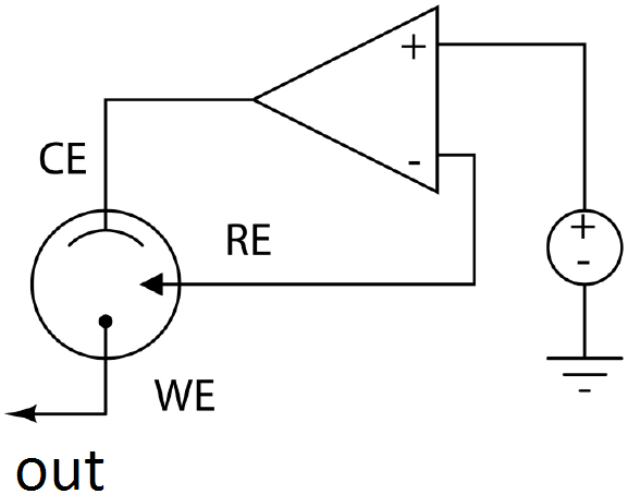

Figure 2.8 Potentiostat System

The popularity of electrochemical sensing stems from its ability to detect a wide range of molecules. These molecules include glucose, Dopamine, Nitric Oxide, and Aminobutyric Acid. The electrical nature of this detection method also makes electrochemical detection a more suitable option for integrated sensors and sensor

arrays. The sensor circuits presented in this work are intended for use in high density electrochemical biosensor arrays, which could be used to provide cellular scale resolution.

NO Electrochemical Sensors

NO electrochemical sensors have been fabricated and utilized to measure NO formation and release from cells, in brain slices, in renal tubule, from the saphenous vein, and in rat hearts. However, the signal transduction mechanisms of NO have not been understood yet. To clarify these mechanisms, the kinetics and localization of NO release and its action targets within a cell need to be studied. This has attracted much interest in the manufacturing of an NO sensor to investigate the NO in single cells or ultrasmall volumes. The ultra-micro-electrodes need to be developed to monitor NO in extremely small spaces in biological microenvironments, such as single cells or certain locations in tissues. The carbon fiber microelectrode with a diameter of several micrometers has great advantages over other electrodes because of its ultrasmall size and large electrode area. In addition, the fast response time (ms – ms) and excellent biocompatibility of the carbon fiber microelectrode make it a powerful tool for the realtime monitoring of biological events. The shape of the carbon fiber microelectrode can be cylindrical, which can offer a high response to NO due to its large electrode area. The shape of the carbon fiber microelectrode can also be a microdisk, which can provide accurate information about the NO concentration at the spot where it is positioned, avoiding the average of the signal as a cylindrical shape. However, the nanometer size of the carbon fiber electrode was only realized by its cylindrical shape.

Modification of NO Electrochemical Sensors

Besides the ultrasmall size of the electrodes that need to be developed, the sensitivity and selectivity should be improved by modifying the electrodes. Malinski and Taha developed a sensitive NO sensor by modifying the carbon fiber electrode with Ni-porphyrin and Nafion and found that Ni-porphyrin had a catalytic effect on the electrooxidation of NO. Since then, many materials have been found to catalyze the NO

electrooxidation and used to modify the electrode for an improvement in sensitivity. Due to their small size and large surface area, nanomaterials such as multiwalled carbon nanotubes (MWNTs), single-walled carbon nanotubes (SWNTs), gold nanoparticles, nanoTiO2, TiO2–Au nanocomposite, nano-alumina, poly-CuTAPc (copper metal tetraaminophthalocyanine), and nano–SnO2 have been widely used as mediators to catalyze the reduction or oxidation of NO. The main role of these nanomaterials as the modifiers of the electrode is to improve the sensitivity and selectivity of the electrochemical detection of NO. Generally, the electrocatalytic properties of nanoparticles can enhance the peak current of NO and lower the potential peak.

Carbon nanotubes have been widely used as scanning probes, batteries, electron field emission sources, nanoelectronic devices, and chemical sensors. Two forms of carbon nanotubes exist: SWNTs and multi-walled carbon nanotubes. Carbon nanotubes can promote electron-transfer reaction when used as an electrode in an electrochemical reaction due to their subtle electronic properties. Furthermore, carbon nanotubes have a high porous structure and small dimension, which provide a new application in the electrode surface modification to design new electrochemical sensors and novel electrocatalytic materials. Both MWNTs and SWNTs have been studied for the electrocatalytic oxidation of NO. An obvious anodic peak at +0.72 V on the cyclic voltammogram of NO is observed on the multi-walled carbon nanotubes modified glassy carbon (GC) electrode with Nafion coating. This is similar to a poly-CuTAPc-modified electrode, which suggests that MWNTs can act as a new electrode material to catalyze the oxidation of NO. The peak current is observed to increase significantly, which may be due to the large surface area and good adsorptive property of MWNTs for NO. The mechanism of NO oxidation at the MWNT-modified electrode is assumed: Nitric oxide is absorbed by carbon nanotubes first, and then it loses an electron to the electrode and NO is oxidized. The MWNT-modified electrode showed a good linear relationship in the NO concentration range of 0.2–150 mL. The detection limit has been estimated to be 80 nM. In order to prepare an ultra-microelectrode for the determination of NO in a biological system, the MWNT-modified carbon fiber ultra-microelectrode was fabricated by Wang et al. to determine NO in liver mitochondria. The oxidation peak potential of MWNT/Nafion-modified carbon fiber is at +0.78 V, with the linearity

of 0.2–86 mM. The MWNT has also been studied with other polymers to enhance electrocatalytic abilities.

Function and Properties of Nitric Oxide

Investigating the properties and function of NO can provide important information with respect to developing methods for determination of NO

Chemical Properties of Nitric Oxide

One of the principal reasons that the chemical biology can be categorized into direct and indirect effects is due to the fundamental chemical properties of NO. It has an odd number of electrons with the unpaired electron in a n_{π}^{*} antibonding orbital; hence, it is a stable radical. NO does not react rapidly with most biological substances (which is in contrast to oxygen radicals such as HO·). Since the in vivo lifetime of NO is relatively short (less than 10 sec), only the faster direct reactions of NO, (such as those with metal centers or other radicals), are likely to be important.

Physical Properties of Nitric Oxide

NOis a colorless gas. The solid and liquid forms exhibit a pale blue color. The solubility of NO is 1.9mM in aqueous solution at 1 atm pressure, and NO has been reported to diffuse at a rate of 50 mm per second in a single direction in biological systems. A simple rule of thumb for the solubility and transport of NO is that these properties are similar to those of dioxygen.

Direct Effects of Nitric Oxide

Direct effects involve the interaction of NO with the chemical or biological target.

1. Nitric oxide reactivity with metals: reactions with metal centers are critical to understand the bioregulatory behavior of NO and why this molecule can serve as a signaling agent. The reaction of NO with some transition metal complexes results in the formation of metal-nitrosyl adducts. NO can react with ferrous ion to form iron

nitrosyl. Hemecontaining proteins are important in the biology of NO, i.e. the reaction between NO and heme cofactors within the protein are important in the regulation of guanylate cyclase activity. NO has been shown to bind to the heme moiety of this protein, thereby stimulating the conversion of GTP to cGMP.

2. The interaction of NO with cytochrome P450: several studies have shown that NO inhibits mammalian P450 which is thought to regulate the hormone metabolism and decrease the drug metabolism in the liver under infectious conditions.

3. The direct reaction of NO with metallo-proteins is a major in vivo control mechanism of NO concentrations. NO reacts with oxy-hemoglobin (HbO2) or oxy-myoglobin to form nitrate and met-hemoglobin (MetHb) or met-myoglobin. This reaction has been proposed as a key mechanism to control NO in vivo:

4.

$$HbO_2 + NO \rightarrow MetHb + NO_3^-$$

The reaction of ferryl heme proteins with NO is important to understand the mechanism of protection against reactive oxygen species by NO.

Literature Review

Electrochemistry is well suited to measuring nitric oxide (NO) in biological fluids because it can detect authentic NO in real time and in situ. In addition, NO electrodes can be made small enough to be used for many applications in vivo. However, there are pitfalls to making reliable electrochemical measurements in any system, especially in complex biological systems. In a previous volume of Methods in Enzymology, we discussed some of the difficulties involved in making such measurements along with strategies for overcoming those difficulties, and we gave the example of measuring NO in circulating blood in vivo (Allen, Liu, & Piantadosi, 2005). The somewhat different challenges involved in measuring NO in biological fluids that are maintained in contact with a gaseous environment, in order to study such processes as the sequestration or release of NO from blood cells as they move between regions of high and low PO2 levels.

The interactions of blood with NO are complex, partly reflecting the nature of blood itself—variously a solution, suspension, and emulsion of cells, lipids, proteins, gases, electrolytes and water—and partly because of the facility with which NO, as a free radical, can coordinate, bond, or react with many other chemical species, particularly with those containing oxygen, transition metals, or sulfur. The physiological consequences of these interactions are also diverse and span extremes: Blood can either destroy or preserve NO biological activity. Thus, a concentrated hemoglobin solution can rapidly extinguish NO biological activity (Allen, Liu, & Piantadosi, 2005). However, within the supporting chemical milieu of the red blood cell, hemoglobin can bind NO and then release it at another time and place, with bioactiv ity inta ct (Pawloski, Hess, & Stamler, 2001). In addition, NO can react with components of the blood to produce other species that have biological activities of their own, such as peroxynitrite and nitrotyrosine (Beckman & Crapo, 1997). Elucidation of the mechanisms by which the fate of NO in the blood is determined is under investigation in a number of laboratories. Of particular interest is the question of how the interaction of red blood cells with NO might be modulated by changes in oxygen content of the blood.

As the blood circulates between the meshwork of capillaries surrounding an alveolus and the capillary bed of intensely metabolizing tissue, its oxygen content may fall fivefold. Typically, the vessels from which gas exchange takes place between the blood and its immediate environment are a few hundred microns in diameter. To illustrate the principles and problems involved in detecting the status of NO in the blood in vitro, we present experimental data from preparations in which an NO-selective electrode was immersed in a drop of heparinized mammalian blood suspended within a flowing and humid gas mixture, which keeps the blood fluid for several hours and allows NO measurements to be made under a wide range of experimental conditions (Allen, Liu, & Piantadosi, 2005).

In 1996, Zhang et al. reported the carbon fiber cone nanometer-sized electrodes with total tip sizes as small as 50 nm. The electrode was fabricated by the carbon fiber etched by an argon ion beam, which has higher mechanical properties than that of the carbon fibers etched by flames. However, the overall physical tip dimensions with large

insulating and supporting electrodes are in the millimeter range and cannot be used for measurement at the single-cell level(Zhang, Zhang, Zhou, & Ogorevc, 1996).

In 2002, Zhang's group reported a nanometer-sized electrode for nitric oxide with a tip diameter of just 100 nm. This NO sensor consisted of a single etched carbon fiber working electrode combined with an Ag/AgCl reference electrode.To prepare this integrated nanometer-sized NO sensor, the carbon fibers are first etched with an argon beam to obtain sharpened tips with diameters ranging from 100 nm to several hundred nanometers. The etched carbon fiber is mounted on the end of a copper wire and fixed by silver epoxy. The mounted carbon fiber silver wire is inserted into a glass capillary and sealed with epoxy. A 1.5-cm Ag/AgCl layer is coated on the tip of the capillary to serve as the reference electrode. Such a design enables a two-electrode configuration to be free in the use of an external reference electrode. Leaving 2 mm of Ag/AgCl exposed at the very tip, the remainder of the Ag/AgCl is coated with insulation and further coated with carbon ink to form a shielding layer. This shielding layer can eliminate the electronic noise and therefore enhance the detection limit to a low-nM range. The sensor tip is dipped into a 3% Nafion solution three times each for 20 s and dried at 90^{o}C for 20 min to form the perm-selective coating membrane. The negatively charged Nafion layer can eliminate the interference of anionic molecules, such as ascorbic acid and nitrite. Furthermore, it can stabilize the NO+ formed upon the oxidation of NO and prevent the formation of nitrite and nitrate. However, Nafion cannot eliminate the interference of cationic molecules such as dopamine, serotonin, and neutral molecules (e.g., hydrogen peroxide, acetaminophen, etc.) (Zhang et al., 2002).

In 2000, the same group reported the use of the hydrophobic WPI coating membrane to improve the selectivity of the microelectrode sensor. The Nafioncoated electrode was immersed in the 5% WPI membrane in acetone solution two times each for 30 s to form the hydrophobic coating layer. The response time is critical for NO sensors for in vivo measurement, since the NO's half-life is on the order of seconds. The thickness of Nafion and the WPI selective membrane, which can decide the diffusion rate of NO, is essential for the response time of the NO nanosensor (Zhang, Cardosa, Broderick, Fein, & Lin, 2000).

Zheng et al. reported that the cofunction of MWNTs–ACB (azocarmine B) and PACB (polyazocarmine) made the oxidation peak current of NO increase greatly. The

MWNT was noncovalently functionalized with ACB and cast onto the glassy carbon electrode. The surface-modified electrode was further covered by PACB via electropolymerization and followed by Nafion solution casting. The differential pulse voltammograms of the obtained Nafion/PACB/MWNT–ACB/glassy carbon electrode showed a much higher peak current compared to Nafion/MWNT/ glassy carbon electrode or Nafion/PACB/glassy carbon electrode. The PACB can decrease MWNT's proton-donor ability and lead to the enhancement of its electrocatalytic ability. The current response of the Nafion/PACB/MWNT–ACB/glassy carbon electrode exhibited an excellent linear relationship with the concentration of NO in the range of 0.22–120 mM. The sensitivity and the determination limit were 0.25 mA/ (mmol/L) and 28 nM, respectively. The sensor also showed good selectivity, stability (95% of its initial response remained after being kept for one week), and reproducibility (parallel detection 10 times, with a relative standard deviation of 2.1%). This sensor was further used for measuring NO released from rat liver cells, and results showed that the sensor could have practical applications in an NO monitoring system (Zheng, Hu, Peng, Yue, & Hu, 2008).

With the goal of designing a biosensor system to meet specific biosensor requirements, one specific area of interest is in the ability to detect the spatiotemporal process of cellular communication. The ability to visualize the molecules of cellular communication allows scientists to further understand the biology that drives normal and pathophysiological processes. Electrochemical sensor arrays provide new opportunities for chemical vision without the addition of labels, such as chromophores or fluorophores. The growing interest in high density electrochemical sensor arrays (Qi et al., 2003; Xu, Lemon, & Liu, 2002).

Research Concept

Investigation of NO electrochemical sensors have been fabricated and utilized to measure NO formation and release from cells

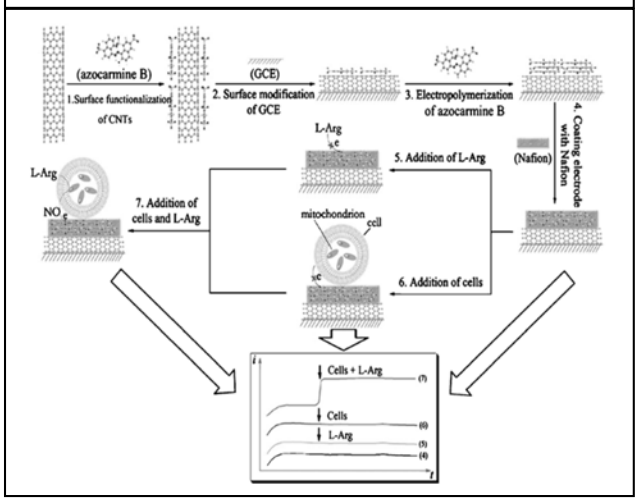

High Sensitivity Nanobiosensor

Electrode

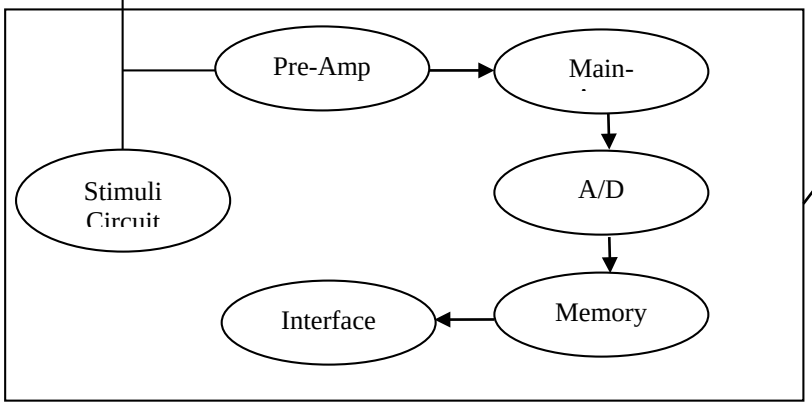

Chapter 3
Research Methodology

Fabrication of Electrochemical Biosensor for Detection of Nitric Oxide by Systematic Review

Materials and Methods

Tetrasulfonated nickel phthalocyanine sodium salt and polyamidoamine (PAMAM) fourth generation dendrimer were purchased from Sigma-Aldrich. The aqueous solutions of NiTsPc and PAMAM were used at concentrations of 0.5 and 1.0 g·L−1 respectively, both at a pH of 4, at room temperature. The pH of the solutions was adjusted using a 0.1 M H2SO4 solution. Dopamine (DA) (3-hydroxytyramine hydrochloride, C8H11NO2·HCl), norepinephrine (NEp), epinephrine (Ep), Uric acid (UA) and the Griess reagent were purchased from Sigma-Aldrich (Steinheim, Germany, www. sigmaaldrich.com/). The concentrations of DA, NEp and Ep used ranged from 1 μM to 500 μM, prepared in a PBS solution, pH 7.4. Ascorbic acid (AA) (C6H8O6), hydrogen peroxide (H2O2), Na2HPO4 x 2 H2O, NaH2PO4 x H2O, NaCl and sulphuric acid (H2SO4) were purchased from J.T.Baker (Griesheim, Germany, www.chemeurope.com/). Sodium nitrite (NaNO2) was purchased from VWR International (Leuven, Belgium, www.be.vwr.com/). Carbon fibers (SIGRAFIL C) with an average diameter of 7 μm were purchased from the SGL Carbon Group (Meitingen, Germany, www.sglgroup.com/).

Carbon-fiber electrodes were produced following a previously reported procedure (Oni et al., 2004). Briefly, a single CF was connected to a copper wire (0.5 mm diameter) using conductive carbon cement then inserted into a borosilicate glass capillary (Hilgenberg GMBH, article number: 1400372, length (100 mm), external diameter (1.5 mm) and wall thickness (0.375 mm). The exposed part of the carbon fiber was coated by an electrodeposition paint and treated in an oven at 180 °C for 20 min to form an insulating layer over the carbon fiber. A carbon disc was exposed by cutting the insulated carbon. The CF had an average diameter of 7 μm which was determined

by cyclic voltammetry using a solution of *Ru (NH3)6]3+/2+ in 5 mM KCl, following the procedure proposed by Marken et al (Hengstenberg, 2001).

Procedure for Fabrication of One Bilayer

Fabrication of one bilayer of PAMAM/NiTsPc on a CF, with PAMAM acting as a polycation and NiTsPc as a polyanion. As a prerequisite for efficient growth of layer-by-layer (LbL) films, parameters such as the pKa of the adsorbed materials have to be considered.

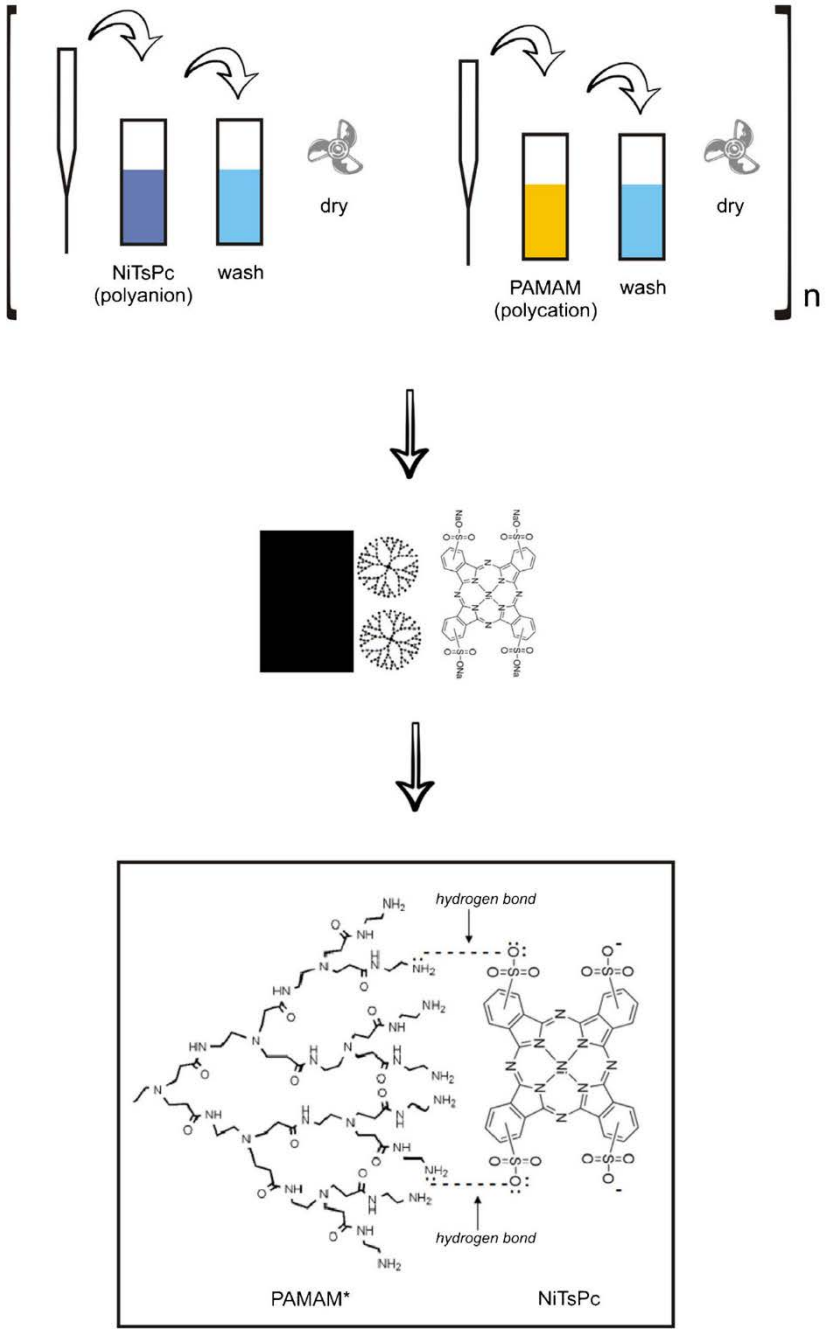

Figure 3.1 Schematic illustration of LbL fabrication of one bilayer

Schematic illustration of LbL fabrication of one bilayer of PAMAM/NiTsPc on a CF, with PAMAM acting as a polycation and NiTsPc as a polyanion. The surface groups of PAMAM and NiTsPc molecules are shown at the bottom of the figure. (*This structure represents a small part of the PAMAM molecule). The back-bonding capability of the metal centres in metallophtalocyanines can be estimated by analyzing

the pKa of the free ligands and the coordination compounds. For example, deprotonation of NiTsPc is expected at pH values above 2.5, one unit above its pKa value, where all the four sulfonic groups are expected to be dissociated. Under such conditions, the SO3 − groups of NiTsPc are expected to interact with the NH3 + groups from PAMAM to form saltbridges. Furthermore, the negative charge of the phthalocyanine rings prevents inter- or intra-molecular aggregation, which makes these molecules suitable to use in LbL assembly. A key feature of the LbL film-formation technique is its ability to produce supramolecular structures whose properties may differ entirely from the bulk properties of the parent materials used to make the films (Alencar et al., 2007; Johnson & Shepherd, 1983).

Electrochemical Measurements

A custom-built electrochemical cell was used to ensure exclusion of oxygen during NO detection. CF modified with PAMAM followed by NiTsPc (CF-PAMAM/NiTsPc) or vice versa (CF-NiTsPc/PAMAM) were used as working electrodes. A Ag/AgCl/KCl in 3 M KCl electrode was used as the reference electrode. Differential pulse voltammetry (DPV) with step size (2 mV), pulse size (50 mV) and pulse time (0.05 s) was used to study the electrochemical properties of the CF-(PAMAM/NiTsPc) sensor, and to evaluate the effect of film thickness on the detection features using electrochemical impedance spectroscopy (EIS). For EIS measurements, an alternating potential with amplitude of 5 mVin the frequency range of 0.1 Hz to 10 kHz was applied to the electrode at open circuit potential, in a buffer solution containing 80 μMofNO. The electrochemical measurements were carried out with a Gamry/potentiostat/galvanostat/FRA (Gamry Instruments, Warminster, DA, www.gamry.com/) having a built-in electrochemical impedance analyzer. Before each measurement, the NO-sensor was placed in 10 mL of a deaerated 0.1 M phosphate buffer (pH 7.4) and cyclically polarized between 0.50 and 1.0 V at a scan rate of 100 mV·s−1 until steady voltammograms were observed (Cancino et al., 2015).

Preparation of NO Solution

Saturated NO standard solutions were prepared by reacting H2SO4 (10 %), added dropwise, with NaNO2 contained in a flask. The preparation was carried out with

strict exclusion of oxygen which was achieved with the help of a vacuum/argon line. The evolved gas was first passed through two troughs of saturated KOH in series for purification, then bubbled at a gentle flow rate into 25 mL of a degassed phosphate buffer (0.1 M) at 4 °C for a minimum of 15 min to ensure NO saturation. Calibration solutions were prepared from the saturated NO standard solutions by serial dilution with the degassed buffer while ensuring strict exclusion of oxygen. The NO standard solution was kept at 4 °C in a tight-capped glass vial with a silicon septum (Wheaton, Millville, USA, www.wheaton.com/). The concentration of a saturated NO standard solution was determined by the Griess test and found to be 3.90±0.42 mM under these conditions. The molar solubility of NO in water is 2.9 mMat 4 °C and 1.9mM at 25 °C. Consequently, the NO calibration standards need to be kept at constant temperature and with the exclusion of oxygen. It is important to note that diffusion, electron transfer rates and layer thickness are impacted by the temperature within the calibration solution (Cancino et al., 2015).

Quantification and Effect of Interferents on NO Detection

The detection and quantification of NO was tested in function of the PAMAM layer. For this, two positions CF-(PAMAM/NiTsPc) and CF-(NiTsPc/PAMAM) were tested to evaluate their suitability for NO sensing. Carbon electrodes without and with NiTsPc and PAMAM layers only were also evaluated to verify if these layers may contributed with the NO detection. For NO-sensor calibration, aliquots of the NO standard solutions were added consecutively to a 10 mL degassed buffer solution in the electrochemical cell. The NO concentrations used ranged from 10 to 80 μM. EIS measurements were used to evaluate the influence of the sensor architecture and NO concentration on the resistance to electron transfer (Cancino et al., 2015).

Common interferents including: NO_2^-, H_2O_2, DA, UA, NEp, Ep and AA were evaluated as possible interferentes to NO detection using chronoamperometric curves at 0.8 V. In this case, the purpose to use the PAMAM-incorporated filmwas to observe if this film was able to act as selective layer to discriminate or even decrease the sensibility of those inteferents, as observed for Nafion® or eugenol films (Cancino et al., 2015).

Nanomaterials-Based Electrochemical Sensors for NO by Systematic Review

Electrochemical sensing has been demonstrated to represent an efficient way to quantify nitric oxide (NO) in challenging physiological environments. A sensing interface based on nanomaterials opens up new opportunities and broader prospects for electrochemical NO sensors. This review gives a general view of recent advances in the development of electrochemical sensors based on nanomaterials. It is subdivided into sections on metal nanoparticles (including gold, platinum and other metallic nanoparticles); semiconductor metal oxide nanomaterials (including the oxides of titanium, aluminum, iron, and ruthenium); and finally nanocomposites (such as those formed from carbon nanomaterials with nanoparticles of gold, platinum, NiO or TiO2). The various strategies are discussed, and the advances of using nanomaterials and the trends in NO sensor technology are outlooked in the final section.

Establishment of Electrochemical Biosensor Circuit

Software Operation

Multisim is the schematic capture and simulation application of National Instruments Circuit Design Suite, a suite of EDA (Electronics Design Automation) tools that helps we carry out the major steps in the circuit design flow. Multisim is designed for schematic entry, simulation, and exporting to downstage steps, such as PCB layout. Multisim’s user interface consists of the following basic elements:

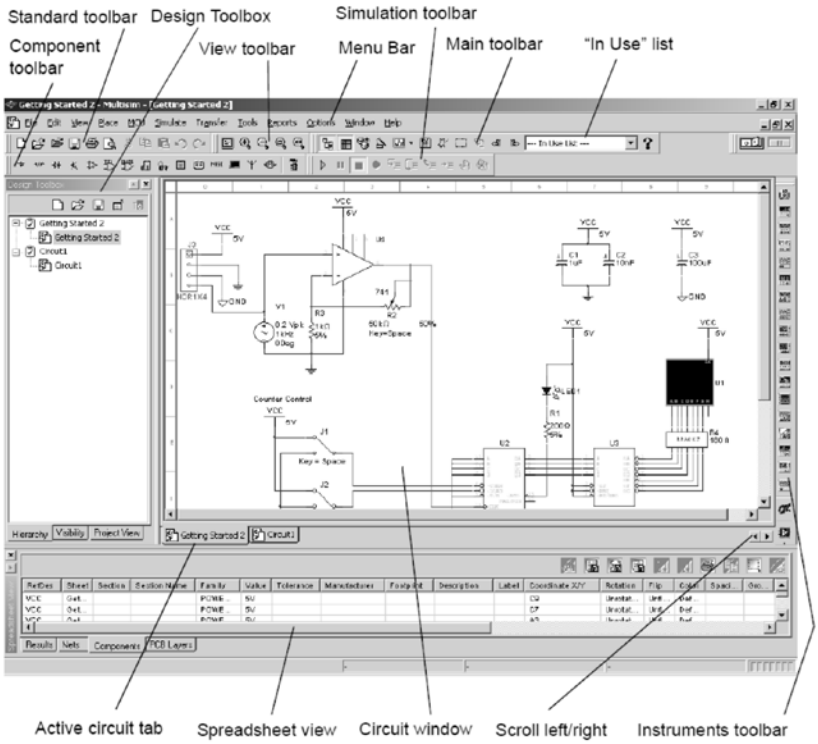

Figure 3.2 Software user interface

Equation Formulation

In a circuit, each common point created by wires and connectors is called a node. The simulator calculates the voltage at each node. Each branch joining two nodes will have a separate current flowing through it. To calculate a circuit solution, a circuit is represented internally as a system of equations, in the form:

$$A*X = B$$

where:

A = modified nodal admittance matrix with dimension *n* x *n*

X = vector of unknowns with dimension *n*

B = vector of constants, also with dimension *n*

n = number of unknowns.

The system of equations is formulated using a general circuit analysis method called the Modified Nodal Approach (MNA). The unknowns (*n)* include each node

voltage (excluding ground), as well as the voltage source currents. B contains the voltage and current source constants, and the entries in the admittance matrix (A) are determined by Ohm’ s law and Kirchhoff’ s current and voltage laws. The modified nodal admittance matrix is deemed sparse because it contains more zeros than non-zeros. Making use of a linked list, the solution of circuit equations can be performed by employing non-zero terms only. This method is called Sparse Matrix Technique. Generally, a sparse matrix approach requires less memory consumption and achieves faster simulation.

Circuit Simulation Methods

Simulation is a mathematical way of emulating the behavior of a circuit. With simulation, we can determine much of a circuit’s performance without physically constructing the circuit or using actual test instruments. Although Multisim makes simulation intuitively easy-to-use, the technology underlying the speed and accuracy of the simulation, as well as its ease-of-use, is complex. Multisim incorporates SPICE3F5 and XSPICE at the core of its simulation engine, with customized enhancements designed by Electronics Workbench specifically for optimizing simulation performance with digital and mixed-mode simulation. Both SPICE3F5 and XSPICE are industry-accepted, public-domain standards. SPICE3F5 is the most recent edition of the SPICE (Simulation Program with Integrated Circuit Emphasis) core designed by the University of California at Berkeley. XSPICE is a set of unique enhancements made to SPICE, under contract to the US Air Force, which include event-driven mixed mode simulation, and an end-user extensible modelling subsystem. Electronics Workbench has further enhanced these cores with certain non-SPICE-standard PSPICE compatibility features to allow for using a wider range of off-the-shelf SPICE models. Multisim’s RF Design module simulates RF circuits using an optimized SPICE engine. There is no need to tell Multisim that your circuit is an RF circuit. RF simulation uses the SPICE simulation engine, but has been optimized to accurately simulate circuits designed to operate at higher frequencies. This optimization uses parts specifically designed and modeled to simulate accurately at these higher frequencies.

After we create a circuit schematic and begin simulation, the solution of the circuit and generation of the data we see on instruments such as the oscilloscope is the role of the simulator. More specifically, the simulator is the part of Multisim that calculates a numerical solution to a mathematical representation of the circuit you created. For this calculation to occur, each component in a circuit is represented by a mathematical model. Mathematical models link the schematic in the circuit window with the mathematical representation for simulation. The accuracy of the component models is one of the key items that determines the degree to which simulation results match real-world circuit performance. The mathematical representation of a circuit is a set of simultaneous, nonlinear differential equations. The main task of the simulator is to solve these equations numerically. A SPICE-based simulator transforms the nonlinear differential equations into a set of linear algebraic equations. These equations are further linearized using the modified Newton-Raphson method. The resulting set of linear algebraic equations is efficiently solved using the sparse matrix processing LU factorization method.

Stages of Circuit Simulation

The simulator in Multisim has four main stages: input, setup, analysis and output.

Input stage- Simulator reads information about your circuit (after you have built a schematic, assigned values and chosen an analysis). This is the process of netlist generation.

Setup stage- Simulator constructs and checks a set of data structures that contain a complete description of your circuit.

Analysis stage- The circuit analysis specified in the input stage is performed. This stage occupies most of the CPU execution time and is actually the core of circuit simulation. The analysis stage formulates and solves circuit equations for the pecified analyses and provides all the data for direct output or postprocessing.

Output stage- You view the simulation results. You can view results on instruments such as the oscilloscope, on graphs that appear when you run an analysis, or in the log file/audit trail.

SPICE-based simulation works by first converting a schematic into a SPICE netlist. Multisim performs this awkward and time-consuming task automatically whenever required. SPICE models are stored in Multisim's extensive parts database. These models are SPICE netlist templates stored in the database. During netlist generation, these templates are expanded for use in the generated SPICE netlist.

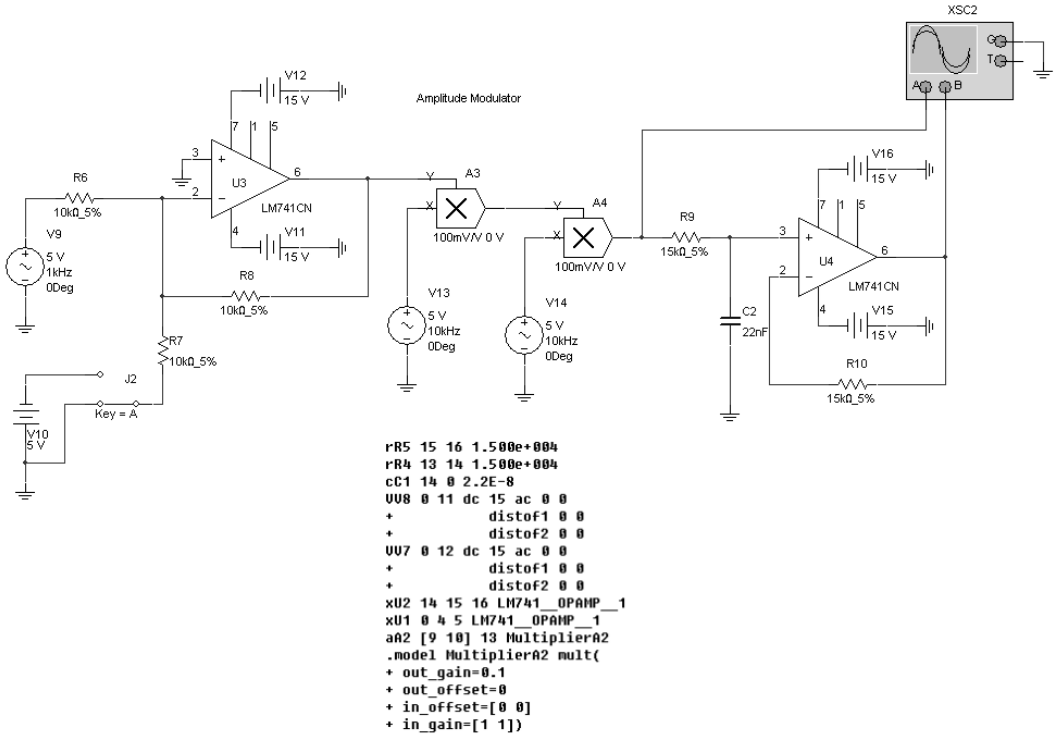

Figure 3.3 Software generates for the amplitude modulator circuit

The text above is a small part of the netlist that Multisim generates for the Amplitude Modulator circuit shown above. This netlist is the actual input to SPICE required to perform the simulation. Prior to the existence of schematic entry programs such as Multisim, designers were required to tediously create such SPICE netlists for themselves each time they wished to analyze a circuit. A modern schematic capture tool, in addition to providing a front-end for PCB layout or other downstream activities such as IC or FPGA design, does this time-consuming and error-prone task automatically. From the netlist, SPICE generates matrices that it solves numerically to come up with voltages (AC and DC) at every node in the circuit. Current *branches* also appear in the matrices when required in order to solve the equations. In particular, current branches appear whenever voltage sources are used (SPICE trick: if you need

to measure a current in SPICE, insert a 0V voltage source. It will not affect the circuit but will force SPICE to compute the current running through the 0V source). For a transient analysis (which is also the basis for interactive simulation), the matrices are solved at every time step in the simulation. Because non-linear analog parts are present in the simulation, at each time step successive approximations are used to compute the final node voltage results. It is possible under certain circumstances that these results will not converge. When this happens, SPICE backs up to 1/8th the time step used previously and tries again.

Digital Simulation

Digital parts are modeled differently than analog parts. Digital parts are connected to the analog parts of the circuit using special XSPICE code models for A-to-D and D-to-A bridges. These models transform voltages into digital events and vice-versa. Thus a net in a schematic may be either analog or digital, but not both at once. When digital parts are connected to one another, the digital events propagate from one to the other with the appropriate simulated time delays. Time steps are automatically inserted into the simulation whenever digital events make their presence felt on the analog parts of the circuit. This event-driven simulation approach to digital simulation allows these types of simulation to run much more quickly than analog simulations (hint: set the simulation parameter Tmax, the maximum analog time step, quite high for digital simulations in order to speed things up dramatically). When simulating circuits with digital components, you have the option of simulating for speed or for accuracy. The “Ideal” option simulates your circuit quickly by not taking into account variances in digital power and internal tolerances. The time to simulate digital components is faster but the signal is not as accurate. The “Real option simulates your circuit accurately, but slower than the “Ideal” option, by accounting for all variances. When using “Real” simulation settings, you are required to add digital power and digital ground to your circuit. To select a digital simulation option for the active design:

1. Choose **Simulate/Digital Simulation Settings** to display the **Digital Simulation Settings** dialog box.

2. Select one of:

· **Ideal**−in this mode, if two digital pins are connected to one another, no additional circuitry is supplied. If a digital pin is attached to an analog node, a simplified pin driver circuit and A-to-D or D-to-A bridge is added into the netlist to smooth the edges of the abrupt digital transitions.

· **Real**−in this mode, all digital pins are attached to D-to-A or A-to-D converters, and more complex pin drivers better representing actual digital pin drivers are inserted into the netlist.

3. Click **OK**.

Chapter 4
Results

Electrochemical Properties of Layered Films for NO Detection

Nitric oxide sensors were constructed by layer-by-layer (LbL) assembly of nickel (II) phthalocyaninetetrasulfonate (NiTsPc) alternated with a polycationic dendrimer (PAMAM) on carbon fiber (CF) microelectrodes. Macrocyclic complexes containing nickel have previously been reported to improve the amperometric detection of nitric acid (Amatore, Arbault, Guille, & Lemaître, 2008; Biesaga, Pyrzyńska, & Trojanowicz, 2000; Malinski & Taha, 1992; Oni et al., 2004). Metalloporphyrins are known to be capable of accommodating additional ligands in their coordination spheres to form a distorted octahedral ligand shell at the central metal (Biesaga, Pyrzyńska, & Trojanowicz, 2000), while NO has also been reported to be capable of interacting with different metalloporphyrins forming adducts in the process (Hoshino, Laverman, & Ford, 1999). The mutual interaction between a porphyrin film adsorbed on an electrode and NO in solution is believed to facilitate the oxidation of NO at the modified electrode. Since porphyrins are structurally and functionally related to metallophthalocyanines, we expect a similar kind of interaction between NO and the metal centre. Jin et al. have proposed that the oxidation of NO on NiTsPc follows the mechanism outlined below (Jin, Miwa, Mao, Tu, & Jin, 1999):

$$[\mathrm{Ni(II)TsPc}] + \mathrm{NO} \rightarrow [\mathrm{Ni(II)TsPc}](\mathrm{NO})$$
$$[\mathrm{Ni(II)TsPc}](\mathrm{NO}) \rightarrow [\mathrm{Ni(II)TsPc}](\mathrm{NO})^{+} + \mathrm{e}^{-}$$
$$[\mathrm{Ni(II)TsPc}](\mathrm{NO})^{+} \rightarrow [\mathrm{Ni(II)TsPc}] + \mathrm{NO}^{+}$$

According to some reports (Souto, de Saja, Gobernado-Mitre, Rodriguez, & Aroca, 1993), formation of an adsorbed adduct is expected to be the initial process during the interaction of oxygen and nitrogen oxide species with metallomacrocyclic complexes, which in this case would be a *Ni (II) TsPc] (NO) adduct, the adsorbed species being subsequently oxidized (Amatore et al., 2008). In the case of PAMAM

molecules, it is know that these molecules are extensively used to encapsulate NO species (Roveda Jr, Papa, Castellano, & Franco, 2014; Stasko & Schoenfisch, 2006). Moreover, PAMAM molecules have been combined with porphyrins to improve the encapsulation process and the release of NO in the drug-delivery concept. We pursued the hypothesis that a similar platform could be used for electrochemical monitoring of NO, that is, to preconcentrate NO species within the dendrimer molecules while the phthalocyanine complex is employed as the electroactive component.

The Influence of the Layered Films in the NO Sensor

In order to evaluate the influence of the PAMAM layer in the NO sensor, the initial step in this study involved investigation of the response to NO of two main architectures, CF-(PAMAM/NiTsPc) and CF-(NiTsPc/PAMAM). Bare CF, CF-NiTsPc and CF-PAMAM were also evaluated to check their contribution in the NO detection. The differential pulse voltammograms (DPVs) and corresponding calibration graphs in Figure below show the responses of the different sensors. The NO oxidation current was highest at about 0.8 V when both NiTsPc and PAMAMwere assembled on the carbon fiber surface (Figure 4.1). The CF-(PAMAM/NiTsPc) sensor outperformed CF-(NiTsPc/PAMAM), and its sensitivity (or slope of the calibration curves corresponding to the sensor architectures employed in Figure 4.1 at concentrations of 0, 16, 24, 32, 40, 48, 60, 80, and 100 μmol in a deoxygenated phosphate buffer at pH 7.4. For DPV measurements, the scan rate was 10 mV s−1, pulse amplitude: 25 mV and pulse width: 50 ms derived from Figure 4.2 (5.54 pAμmol^{-1})) in the linear range of 16 to 80 μmol was twice as high as that for CF-(NiTsPc/PAMAM) (2.71 pA μmol^{-1}) which was linear in range of 24 to 100 μmol.

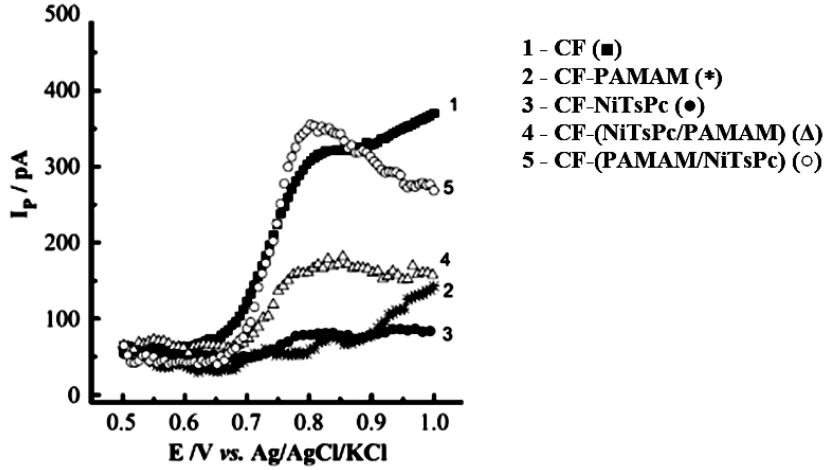

Figure 4.1 The differential pulse voltammograms obtained with different NO sensor architectures at a NO concentration of 60 μmol

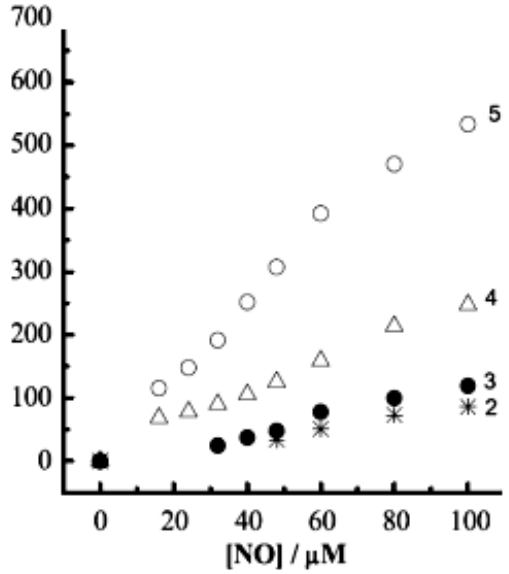

Figure 4.2 Calibration curves corresponding to the sensor architectures employed in A at each concentration

The position of PAMAM molecules in the layer formation influenced the sensor performance, especially in terms of current, changing current values from 174pA to 357pA for CF-(NiTsPc/PAMAM) and CF-(PAMAM/NiTsPc), respectively. The better performance of the CF-(PAMAM/NiTsPc) sensor compared to CF-(NiTsPc/PAMAM) may be caused by a favourable structural organization of PAMAM and NiTsPc groups

at the carbon fiber surface. The large PAMAM film at the interface with the electrolyte may affect the diffusion of NO, while the PAMAMmolecule between NiTsPc and carbon fiber may concentrate *Ni (II) TsPc] (NO) adduct species formed in the first film composed by NiTsPc. Since PAMAM is not electroactive, any electrochemical processes expected from the CF-(PAMAM/NiTsPc) films should arise from the interaction of the metallophthalocyanines with NO.

The electron transfer properties across the layer-by-layer films

In order to understand the observed characteristics of the sensor architectures in more detail, electrochemical impedance spectroscopy (EIS) measurements were carried out to elucidate electron transfer properties across the LbL films. The results of which are shown by means of the Nyquist plots in Figure 4.3. A particular advantage of characterizing electron-transfer processes across microelectrodes using AC impedance spectroscopy is that the diffusional impedance is significantly reduced compared to that observed at normal electrodes. The Nyquist plots were recorded at 0.80 V using an ac perturbation voltage of 0.005 V in the frequency range from 0.1 Hz to 10 kHz in a degassed buffer (phosphate buffer pH 7.4) containing 60 μM of NO. There were significant differences in the electron transfer resistances of all the modified films compared to unmodified CF as shown in Figure 4.3.

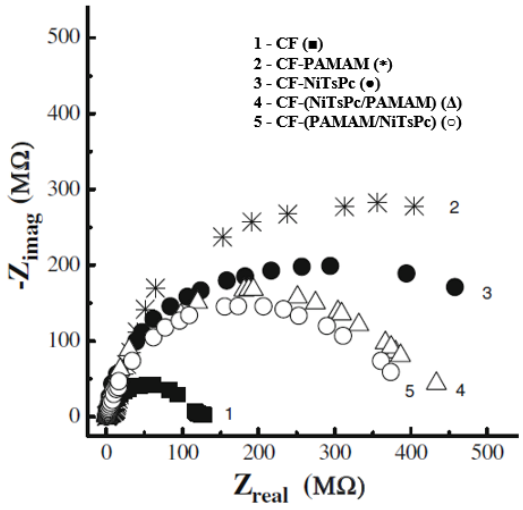

Figure 4.3 Nyquist plots obtained for a non-modified

The charge transfer resistances derived from the EIS measurements could be correlated with the results of the corresponding DPV (Figure 4.1 and 4.2). The CF-PAMAM sensor had the highest electron transfer resistance compared with the other sensors, and was also associated with the highest capacitive behaviour. This is not surprising due to the highly charged nature of PAMAM molecules. The maximum value of the imaginary part of impedance, −Zimag of the CF-PAMAM sensor (300 MΩ) was at least six times larger than that for the bare CF electrode (50 MΩ). The value of the charge transfer resistance for CF-(PAMAM/NiTsPc) (140 MΩ) was 47%lower than that for CF-PAMAM (300MΩ). This implies that the electrostatic interaction between the PAMAM and NiTsPc leads to significant charge neutralization of PAMAM. A decrease in the capacitive behaviour of the film was observed, along with a corresponding decrease in the electron transfer resistance across the film. More justification for this hypothesis may be adduced by a deeper analysis of the EIS results of the CF-(NiTsPc/PAMAM) film. When the architecture of the films is changed in a way that PAMAM interfaces between the bulk electrolyte and the electrode, the charge transfer resistance increases significantly compared to the previous case. We believe that electrostatic interaction of the inner surface of PAMAM with NiTsPc neutralizes some of its charges, while the other surface which is exposed to the electrolyte is unaffected. This indicates that the increase in the capacitive behaviour of the CF-(NiTsPc/PAMAM) film arises from its surface charge. The charge transfer resistance is reduced for the CF-(PAMAM/NiTsPc) film compared to CF-(NiTsPc/PAMAM) due to partial neutralization of the positive charge on PAMAM by NiTsPc. On the other hand, the results also suggest that PAMAM may act like an inhibitory layer to the diffusion of NO+ but not for the formed adduct *Ni (II) TsPc] (NO). This explains the low voltammetric currents observed in Figure 4.1 and 4.2 for the CF-PAMAM. Therefore, the CF-(PAMAM/NiTsPc) architecture acts as the most efficient NO sensor tested in this study, facilitating faster electron transfer compared to the others modifications.

Based on the observed correlation between EIS and DPV results, we suppose that EIS may potentially serve as an alternative technique for NO detection. This concept is not entirely new. Cheng et al. demonstrated that protein polymorphisms can be identified by the charge transfer resistance ratio of the protein-bound electrode from

EIS measurement. The authors proposed that a simple detection method based on measurement of relative charge transfer resistance ratio by EIS was a potential approach for investigating polymorphism due to changes in molecular weight.

The Performance of Sensor Electrode

The performance of CF-(PAMAM/NiTsPc) electrode was further optimized with respect to the number of bilayers. EIS (Figure 4.4 A) and DPV data (Figure 4.4 B) confirm that a sensor with only one bilayer has the most optimal properties, exhibiting both the least charge transfer resistance and the highest oxidation current at 0.8 V. Increasing the thickness of the CF-(PAMAM/NiTsPc) film increases its electron transfer resistance and consequently decreases the oxidation current. Since the PAMAM dendrimer is not electroactive, the decrease in current with film thickness can be attributed to decline in the rate of diffusion of NO across the films to form *Ni (II) TsPc] (NO) adducts for the electrochemical detection.

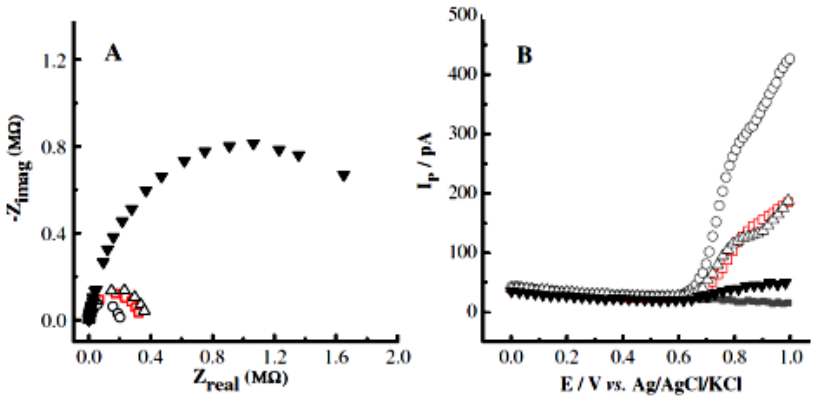

Figure 4.4 (A) Nyquist plots, and (B) DPVs of: background (■), a unmodified carbon fiber (□), and after modification with 1 (○), 2 (Δ) and 3 (▼) bilayers of CF-(PAMAM/NiTsPc)

A typical calibration curve for a CF-(PAMAM/NiTsPc) sensor was obtained from DPVs based on the oxidation currents at 0.80 V, as observed in Figure 4.2. A linear correlation with a correlation coefficient (R) of 0.9732 was obtained in the concentration range from 8 to 80 μM of NO. The sensitivity of the sensor determined

fromthe slope of the regression line was found to be 5.54 pA·μM−1, which compares reasonably to the sensitivity of electrochemical NO sensors previously reported , although significantly higher sensitivities have also been reported . The limit of detection (LOD) of the sensor, determined as the concentration corresponding to a signal to noise ratio of 3:1 was found to be 5.5 μmol. This is substantially lower than the LOD reported for some NO sensors, thus suggesting the need for further optimization of the sensor, especially for NO quantification in a biologically relevant context.(For EIS, the applied potential was 0.80 V, the ac amplitude was 5 mV, and the frequency range was 0.1 Hz to 10 kHz. For DPV measurements, the scan rate was 10mVs−1, pulse amplitude: 25 mV, pulse width: 50 ms.The electrolyte was a deoxygenated 0.1 mol phosphate buffer (pH 7.4) containing 60 μmol NO)

The comparison of the response of sensor

A particularly novel aspect of this study is the use of EIS to successfully characterize NO sensors, especially the possibility to linearly correlate EIS data with the concentrations of NO by means of calibration graphs.

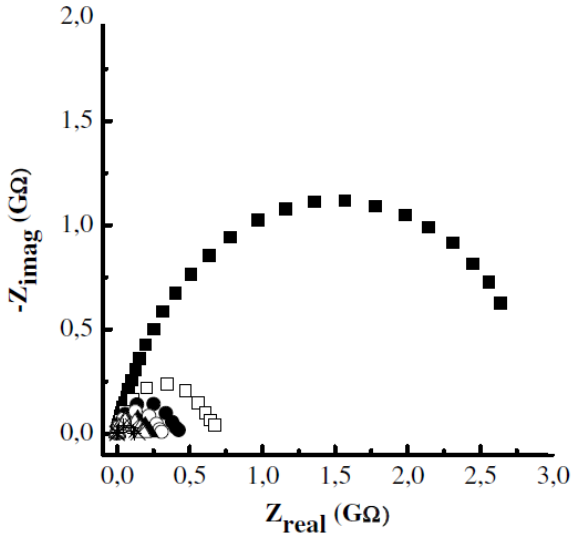

Figure 4.5 Nyquist plots obtained for a modified carbon fiber CF-(PAMAM/NiTsPc) electrode with different NO concentrations of 8 (■), 16 (□), 24 (●), 32 (○), 40 (▲), 48 (Δ), 60 (x) and 80 (+) μmol

Figure 4. 5 shows a typical case for comparison of the response of CF-(PAMAM/NiTsPc) at 0.8 V to different NO concentrations in the range from 8 to 80 μmol by means of Nyquist plots. The electron transfer resistance of the CF-(PAMAM/NiTsPc) sensor was observed to decrease upon increasing NO concentrations. The linear decrease in electron transfer resistance at a fixed potential (0.8 V) could be attributed to the oxidation reaction between NO and NiTsPc rather than due to pure physical adsorption. Determination of NO concentration by monitoring the change in charge transfer resistance of the NO sensing films therefore provides a novel and feasible solution to complement traditional DPVand amperometric measurements (The applied potential was 0.80 V, the ac amplitude was 5 mV, and the frequency range was 0.1 Hz to 10 kHz. The electrolyte was a degassed 0.1Mphosphate buffer (pH 7.4)).

The stability of the NO sensor

The stability of the NO sensor was tested by recording repetitive DPV measurements as shown in Figure 4.6 (in a deoxygenated 0.1 mol phosphate buffer (pH 7.4) containing 60 μmol NO). At least 90 % of the current is retained after 8 consecutive runs. Note that even with this diminished response, the biosensor still has enough sensitivity to be used in NO analysis, especially when used as disposable device. The decline in current is possibly caused by the binding interactions of the NO species on the LbL film at the electrode surface.

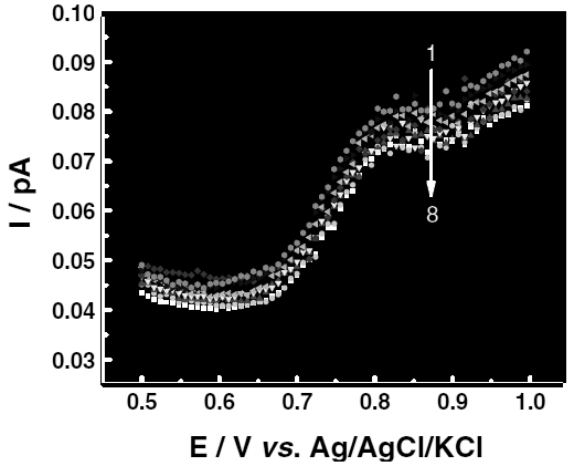

Figure 4.6 Stability graph of the CF-(PAMAM/NiTsPc) electrode

The determination of NO in biological samples suffers from a number of interfering chemical species. The most notable of these include: hydrogen peroxide (H2O2), nitrite anions (NO2 −), dopamine (DA), ascorbic acid (AA), uric acid (UA), epinephrine (EP) and norepinephrine (NEP). H2O2 and NO2 − are particularly troublesome for electrochemical detection of NO since they are oxidized at about the same potential where the oxidation of NO takes place. From the values of the selectivity ratios, the ratio of the detection limit of the sensor to the intereferent to it detection limit against the nitric oxide, the sensor can be seen to have very low selectivity against DA andNEP.However, the catecholamines (DA, EP and NEP) are oxidized at much lower potentials and may thus be easily discriminated through a selective two-step chronoamperometric procedure. On the contrary, the sensor shows impressive selectivity against UA, EP, AA, NO2 – and H2O2. The sensor would only be able to detect these species when their concentrations are in the millimolar range. Since the selectivity of PAMAM against anions is based on electrostatic entrapment, the major challenge of measuring NO in the presence of NO2 − would be the contribution of the background current to the measured signal. A high background was observed upon successive addition of sodiumnitrite to the CF/PAMAM/NiTsPC sensor at 0.80 V, Electronic Supplemenatry Material (ESM). The increase in the background current is due to charge accumulation in the double layer region and on the sensor surface resulting from entrapment of the negatively charged NO2 − ions by the positively charged PAMAM layer.

Selectivity of the NO sensor

For the present sensor, the minimum amount of NO2 − necessary to give a faradaic current is as high as 1.2 mmol, compared to only 5.5 μmol for NO. This study suggests that a LbL configuration can also be successfully used to diminish the interference of several interferents during the detection of NO as shown in Table 4.1 However, the mechanism through which this is achieved is still a subject of investigation.

Table 4.1 Selectivity of the sensor against some of the common interferents during NO detection

Interferent	Sensitivity ($nA \cdot \mu mol^{-1}$)	Selectivity ratio±SD
Nitrite anions($NO2^-$)	7.50×10^{-3}	236±11
Hydrogen peroxide(H2O2)	1.08×10^{-3}	1449 *
Dopamine (DA)	1.86×10^{-3}	45±5
Ascorbic acid (AA)	1.08×10^{-3}	2209 *
Uric acid (UA)	1.45×10^{-3}	739±13
Epinephrine (EP)	2.26×10^{-3}	495±29
Norepinephrine (NEP)	2.18×10^{-3}	40 *

* indicates that the standard deviation was insignificant compared to the mean values. The selectivity ratio was calculated as the ratio of the detection limit of the sensor towards the intereferent to its detection limit towards nitric oxide

The sensor exhibited a selectivity as good as, or even better than similar metalloporphyrin- or metallophthalocyaninebased sensors reported in the literature, where Nafion™, eugenol or some other membrane materials were used to enhance selectivity. Further studies are however necessary to evaluate the robustness and mechanical resistance of this sensor for in vitro and in vivo applications.

Materials and performance characteristics of NO sensors

Metal nanomaterials

Compared with other nanomaterials, metal nanomaterials show excellent characteristics of electronic and catalytic. The synthesis of nanostructures can be achieved by the reduction of precursor metal salts usage reducing and stabilizing reagents. Recently, metal nanomaterials, such as gold nanoparticles, platinum nanoparticles were synthesized and designed to controllably release NO. However, achieving control over the growth of nanostructures leading to proper dimensional confinement and the promising applications in NO sensors is a challenging task. Noble metal nanomaterials have been extensively utilized in different fields in recent years.

Owing to their fascinating electrocatalytic properties, gold nanoparticles (AuNPs) have received the most attention in the fabrication of NO sensors. The AuNPs used in NO sensor are commonly immobilized in various substrates, such as self-assembled monolayer, conducting and non-conducting polymers. For instance, Kannan and John prepared a fused spherical AuNPs modified indium tin oxide (ITO) electrode by the layer-by-layer selfassembly technology. The AuNPs were self-assembled on a (3-mercaptopropyl)-trimethoxysilane sol–gel film, which was preassembled on ITO electrode. The AuNPs modified ITO electrode displays high sensitivity and excellent selectivity towards the determination of NO. The detection limit of the NO sensor is as low as 0.31 nmol·L−1, and the linear range is also wide (12 nmol·L−1 - 0.7mmol·L−1). Yu et al. prepared polyelectrolyte/AuNPs hybrid sensing films by incorporating 4-(dimethylamino) pyridine-stabilized AuNPs into polyelectrolyte multilayers preassembled on ITO electrode, which can be exploited to utilize the films for the electrochemical detection of NO. VinuMohan developed a NO sensor by coating AuNPs dispersed poly (2-(2-pyridyl) benzimidazole) film on GCE, which was successfully applied for the detection of NO released from the living tissues. Thangavel and Ramaraj prepared a Nafion-AuNPsmodified electrode by infiltrating the gold nanostructures into the Nafion matrix. The Nafion-AuNPs-modified electrode showed high sensitivity for NO detection with the detection limit of 1 nmol·L−1. Zhang and Oyama reported an AuNPs array, which can grow on nanostructured ITO electrode by seed-mediated growth approach and can be used for the determination of NO. Li et al. prepared AuNPs monolayer films by the assembly of AuNPs in aqueous colloid at toluene/water interfaces, which can be transferred onto GC surface to assemble bilayer films for electrochemical and catalytic studies. The transferred AuNPs film exhibits a satisfying sensitivity toward NO detection. Zhu et al. found that AuNPs -based platinum microelectrodes exhibited excellent catalytic activity toward NO. We fabricated a novel gold fiber microelectrode based on the growth of AuNPs films onto quartz fibers by a simple chemical liquid deposition. Fig. 3 (left) is the SEM images of the AuNPs on the quartz glass fiber. After the modification by electropolymerized niacinamide and Nafion, the result NO microsensor exhibited high sensitivity and low-detection limit of 3.6 nmol·L−1 (Fig. 3 (right)), and was successfully employed in vivo detection of NO release from mice liver.

Platinum nanomaterials represent another type of metal nanomaterials recently suggested as a catalytic coating for fabricating NO sensors. Yap and coworkers [118] reported an amperometric nitric oxide sensor based on nanoporous platinum phthalocyanine modified electrodes. A two-step synthetic protocol was adopted to provide three Metallo 4′, 4″, 4‴, 4⁗ tetra-amine phthalocyanine complexes by using a laboratory microwave reactor. The PtTAPc product s were electropolymerized within the pores of anodisc nanoporous alumina membrane as a densely packed array of poly-PtTAPc nanotubes. Fig. 4 show the images and schematic diagram of the densely packed array attached to the Pt substrate after dissolution of the anodic aluminum oxide (AAO) membrane, in which the surface area enhancement provided by the nanotube-arrayed morphology enabled a high signal to background current during NO electro-oxidation. The reported sensitivity of the NO sensor based on the modified nanoporous electrode (8.84 μA/μmol·L^{-1}) is higher than that on the modified flat electrode (0.57 μA/μmol·L^{-1}).Wang and Lin developed an electrochemical sensor for sensing NO by electrodeposition of Pt–Fe (III) nanoparticle on a GC electrode. This sensor exhibits excellent electrocatalytic activity for the oxidation of NO. The linearity range of the sensor is between 8.4×10−8 and 7.8×10^{-4} mol·L^{-1} and the detection limit is 1.8×10^{-8} mol·L^{-1} (s/n=3). Xian developed a novel amperometric NO microsensor, which is prepared by electrodeposition of copper–platinum microparticles on the surface of a carbon fiber (CF) electrode. The microsensor was successfully applied to the in vivo determination of NO release from the rat heart.

Copper nanomaterials can be stabilized by cysteine on ITO electrodes with (3-mercaptopropyl) trimethoxysilane. The obtained copper nanoparticles modified electrodes showed high electrocatalytic activity to the reduction of nitrite and NO, which may find its promising application as an electrochemical NO sensor.

Table 4.2 shows the comparison of the performances of the NO sensors based on different metal nanomaterials. Obviously, NO electrochemical sensor based on AuNPs exhibits higher sensitivity and lower detection limit than other metal nanomaterials. It may be attributed to the excellent conductivity and high electrocatalytic activity of AuNPs. It's worth mentioning that the anodic peak of AuNPs appears at about 0.8 V, which is close to that of NO (about 0.7 V), the anodic peak current of NO would be interfered by AuNPs when voltammetry was engaged. So

amperometry should be selected or NO should be detected via its electro-reduction for NO electrochemical sensor based on metal nanomaterials.

Table 4.2 Materials and characteristics of NO sensors based on metal nanomaterials

Nanomaterials	**Substrate Electrode**	**Permeable Membrane**	**Detection limit (nmol·L^{-1}); sensitivity**	**Linear range (µmol·L−1)**	**Selectivity ratio±SD**
PtNPs	GC	DHP	50	0.18–120	NO2−, DA, AA, UA
Cu-Pt	CF	Nafion	30	0.08–4.8	NO2−, DA, AA
Pt-Fe (III)	GC	Nafion	18	0.084–780	NO2−, DA, AA, H2O2,
poly-PtTAPc nanotube/AAO	Pt	Nafion	-	0.01–0.1	-
AuNPs/PNA	Quartz fibers	Nafion	3.6	0.0072–18	NO2−, DA, AA, UA, L-arginine
AuNPs	Pt	Nafion	50	0.1-40	NO2−
AuNPs	GC	toluene/water interface	27	0.05-10	
AuNPs/PPBZ	GC	-	3.7;6.45 A/mol·L^{-1} •cm^2	0.017–2.6	DA, AA
FAuNPs	ITO	Nafion	0.31	0.012–700	NO2−, DA, AA,

AuNPs	ITO/GC	Nafion	1	-	UA, DL-cysteine -

Semiconductor Nanomaterials

Semiconductor metal oxide material, such as SnO2, Bi2O3, Cr2O3, WO3, ZnO and TiO2 is often used as a selective sensing material for NO gas detection. In fact, semiconductor nanomaterials can also be employed to detect NO in solution. Our group employed Al2O3and TiO2 to modify GC electrode. These modified electrodes were found to display an electrocatalytic activity toward NO oxidation with high selectivity and sensitivity. α-Fe2O3 nanoparticles [130] were reported to be prepared by a simple solution-combusting method and dispersed in chitosan solution to fabricate nanocomposite film on GC electrode. The resulted nanocomposite bioelectrode has response time of 5 s, linearity as 5.0×10−7 to 15.0×10−6 mol· L−1 of NO with a detection limit of 8.0×10−8 mol·L−1 and a sensitivity of −283.6 μA/mmol·L−1. Kim et al. [131] reported the application of single crystalline RuO2 nanorods grown on a single carbon fiber as a microsensing device for in vivo NO detection in rat brain. The representative SEM image is shown in Figure 4.7 (right). The dynamic current response of RuO2 nanorods-carbon fiber to the successive increase of NO concentration shows the high sensitivity of the microsensor, which is ca. 40-fold higher than that of bare carbon fiber (Figure 4.7 (left)) Table 4 shows the performances of the NO sensors based on different semiconductor nanomaterials. Carbon material electrode is often used as the substrate electrode for the class of NO sensors. The semiconductor nanomaterials are fascinating because of their selective sensing for NO.

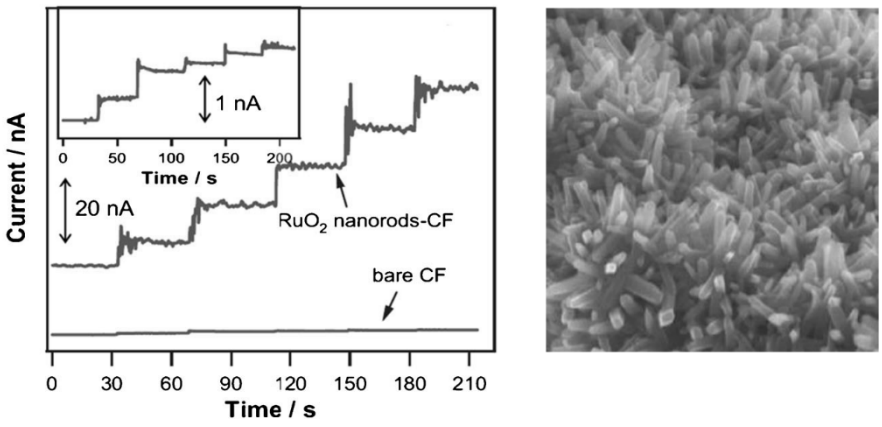

Figure 4.7 Dynamic current responses of RuO2 nanorods-CF and bare CF (left). SEM image of as grown single crystalline RuO2 nanorods on a single carbon fiber microelectrode (right)

Table 4.3 Materials and characteristics of NO sensors based on semiconductor nanomaterials

Nanomaterials	**Substrate Electrode**	**Permeable Membrane**	**Detection limit (nmol·L^{-1}); sensitivity**	**Linear range (µmol·L−1)**	**Selectivity ratio±SD**
RuO2-nanorods	Carbon fiber	-	36.3 nA/µmol·L^{-1}	-	NO2−, DA, AA, H2O2
nano-α-Fe2O3	GC	-	80 nmol·L^{-1}; 283.6 µA/mmol·L^{-1}	0.5–15	-
nano-TiO2	GC	Nafion	54 nmol·L^{-1}	0.36–54	NO2−, DA, AA
nano-Al2O3	GC	-	7.2 nmol·L−1	0.04–210	-

Transimpedance Amplifier Iteration Results

Due to a lack of necessary input and output pins, the independent resistive TIA was attached to the pad using a set of analog switches. These switches were put in place so that the pins could be shared between multiple circuits. Since the circuit was run at a 900mV supply voltage with a 450mV common mode voltage, a voltage-boosting circuit similar to the clock booster circuit to turn the switches on.

No visible response to a current input could be seen from the standalone resistive TIA. The output consisted of clock noise, possibly indicating that the switched

capacitor common-mode feedback circuit was operating. This could be explained by the circuit's input not being physically connected to the input pad, or the outputs not being properly connected to the output pad through the pin-sharing circuitry.

An additional copy of the resistive TIA, which was attached to the main amplifier and sigma-delta ADC, was also fabricated. A sinusoidal input current was generated using a function generator and a resistor, and applied to the input of the TIA. The main amplifier and modulator response to the sinusoidal current input are shown in Figure 4.8.

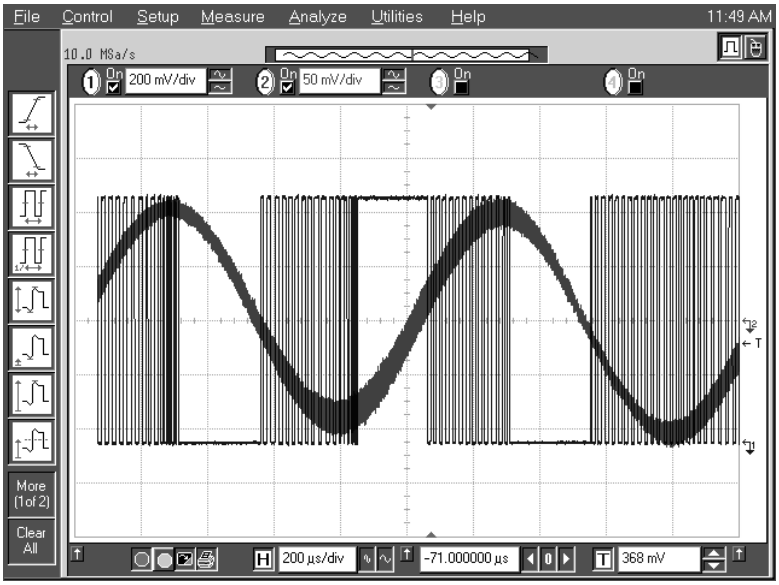

Figure 4.8 Main amplifier and modulator response to sinusoidal TIA input

The Single Ended Switched Capacitor Transimpedance Amplifier

The input current mirror, shown in Figure 4.9, is a high impedance p-type mirror, which allows us to create sub-µA magnitude currents without a high-precision bench-top current source. The current mirror output was also attached to an external pad, to allow the input mirror to be bypassed if a small-magnitude current mirror became available. Due to the resolution of the equipment used to measure the output signals from the TIA, as well as noise from the test bench, the small voltage output generated with a 10nA signal could not be seen. In order to more easily measure the output voltage, the input current was increased.

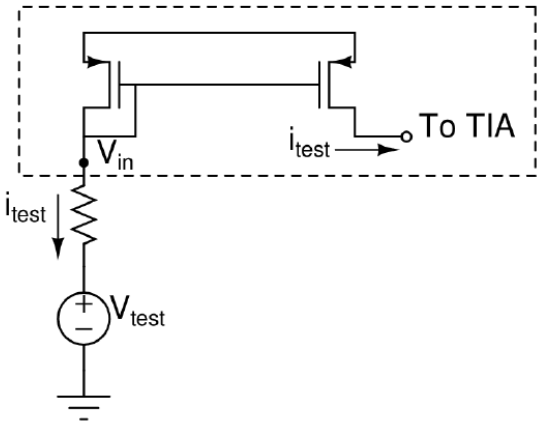

Figure 4.9 Input current mirror schematic

The circuit was tested with a 100nA input current and initially run at the designed clock speed of 1MHz. The measured output is shown in Figure 4.10. During testing, the output showed large amount of switching noise, as well as a voltage step that is hypothesized to be effects of charge injection. This noise could also be attributed to instability in the overall feedback network. The signal peaks at about 20mV at the end of the integration phase, indicating that the circuit achieves an overall transimpedance gain of about 200kΩ.

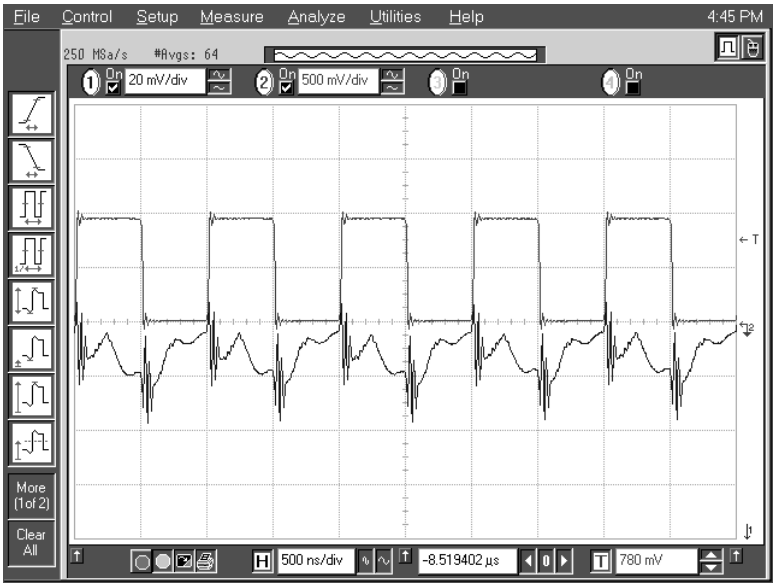

Figure 4.10 Response to a 100nA DC current at 1MHz clock

With a traditional switched integrator design, the clock speed can be slowed down, increasing the gain proportionally. When the clock rate was reduced to 500 kHz, the circuit's output indicated an increase in the overall transimpedance gain of about 2x.The Circuit's response to the same 100nA input current while running at 500 kHz is shown in Figure 4.11.

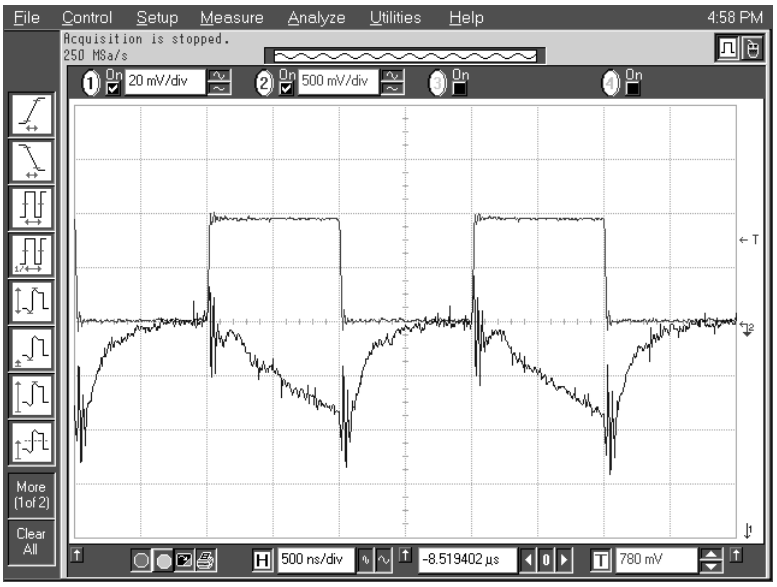

Figure 4.11 Response to a 100nA DC current at 500 kHz clock

At 500 kHz, the magnitude of the switching and charge injection noise appears to be the same, but the circuit now has more time to integrate a larger amount of charge before resetting. With the slowed clock, the circuit achieves a gain of approximately 350kΩ. To further test the circuit's functionality, the input current was increased to 300nA. With the increased input current, the peak response increased to approximately 100mV. This corresponds to a gain of approximately 330kΩ, which is appropriate for the amount of voltage swing occurring at the circuit's output.

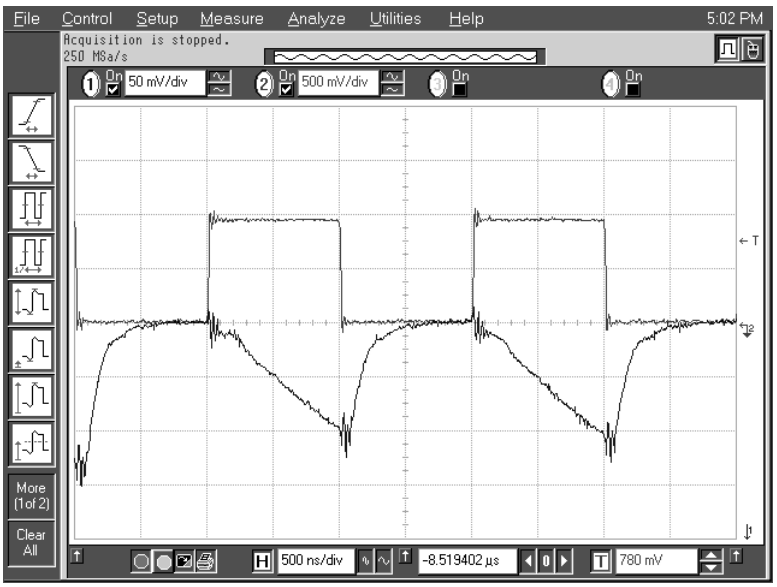

Figure 4.12 Response to a 300nA DC current at 500 kHz clock

Pseudo Differential Transimpedance Amplifier

To start, the circuit was tested with a 10nA input current at a 1MHz clock rate. Both outputs appeared to consist primarily of clock noise. This output is shown in Figure 4.13.

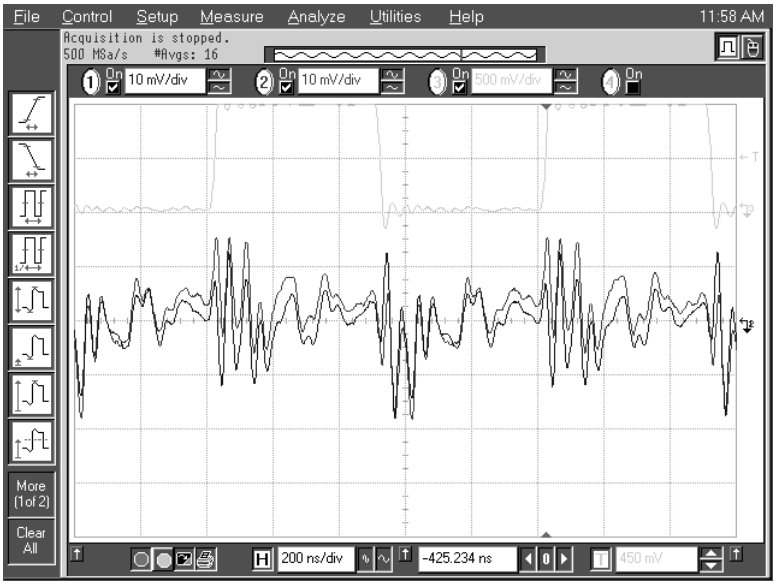

Figure 4.13 TIA response to 10nA input current at 1MHz clock rate

When the circuit's clock rate was reduced to 500 kHz, a difference started to appear between the integration and reset phases. The output from the circuit running at 500 kHz is shown in Figure 4.14.

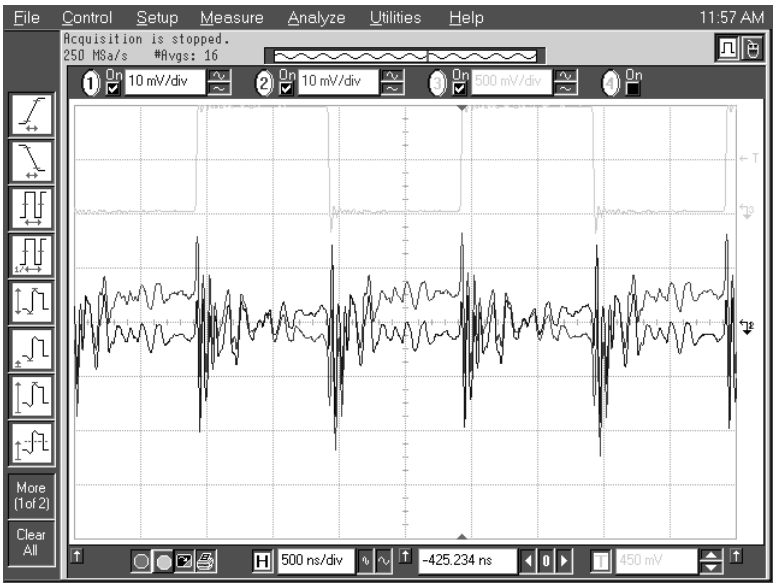

Figure 4.14 TIA response to 10nA input current at 500 kHz clock rate

The output magnitude was still too small to accurately measure the gain, so the clock was further slowed to 200 kHz. At this frequency, the circuit's response to a 10nA signal was clearly visible. The integration of a 10nA DC current resulted in a 20mV differential peak at the end of the integration phase, as shown in Figure 4.15. A 20mV peak with a 10nA input current corresponds to a transimpedance gain of 2MΩ at 200k Hz. Assuming the transimpedance gain scales inversely proportional to operating frequency, 2MΩ at 200 kHz corresponds to a differential transimpedance gain of 400kΩ at a 1MHz clock rate.

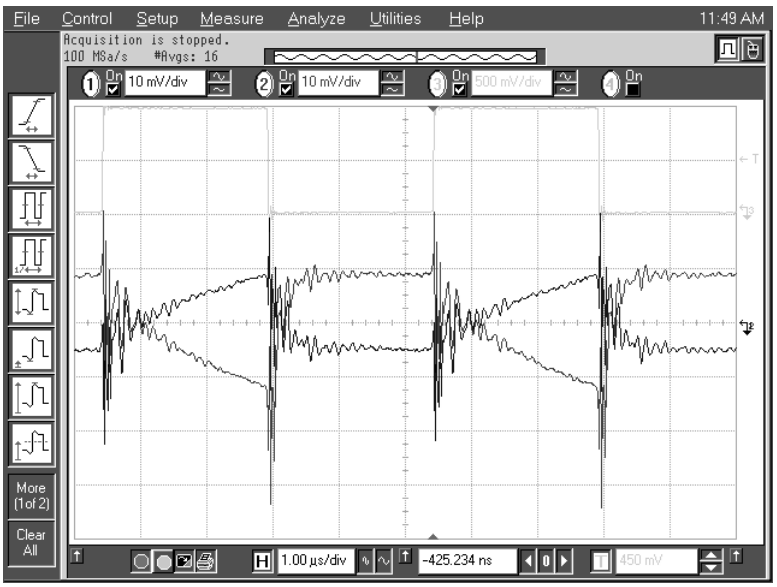

Figure 4.15 TIA response to 10nA input current at 200 kHz clock rate

The overall circuit appears to function similar to the single-ended circuit. In the oscilloscope outputs shown throughout this sub-section, common mode switching noise is apparent. Additionally, there appears to be issues with the two outputs not resetting to the same value during the reset phase, as well as a DC error during the integration phase. These issues can be attributed. To op-amp offset, and effects of process variation on the current mirror output.

Differential Transimpedance Amplifier with Bottom Plate Sampling

Testing of the differential TIA showed that the circuit was functioning, but the gain and output parameters were far from ideal. Throughout the layout and testing process, the device was shown to be very sensitive to parasitic capacitances and asymmetric routing. To begin testing, zero input current was attached to the input of the current mirror. The results of zero current input gave a differential voltage of approximately 10.68mV at the end of the integration phase. The response to zero current input is shown in Figure 5-17.

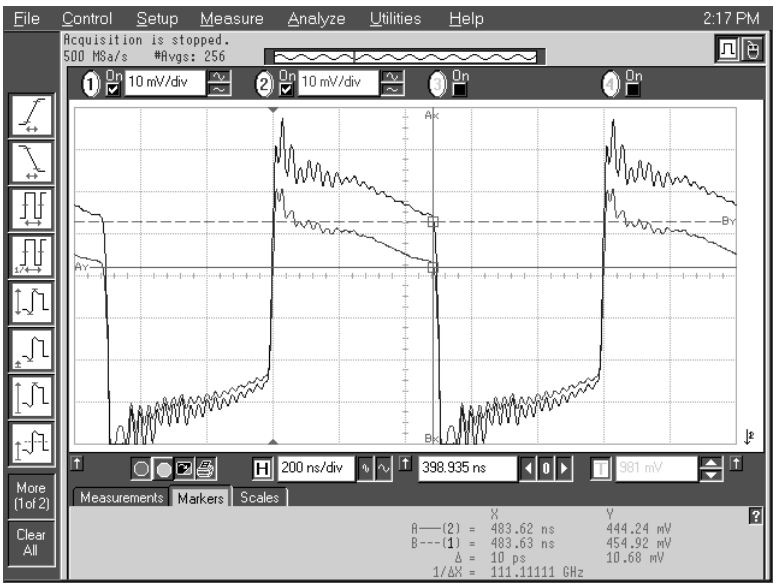

Figure 4.16 Zero input current response at 1MHz clock rate

To test the response of the circuit to a positive input, a 300nA DC current was applied to the input of the current mirror. The measured output is shown in Figure 4.17. A 300nA DC input caused a differential output change of approximately 27.9mV. This change corresponds to a transimpedance gain of only 93kΩ, as opposed to the designed 3MΩ.

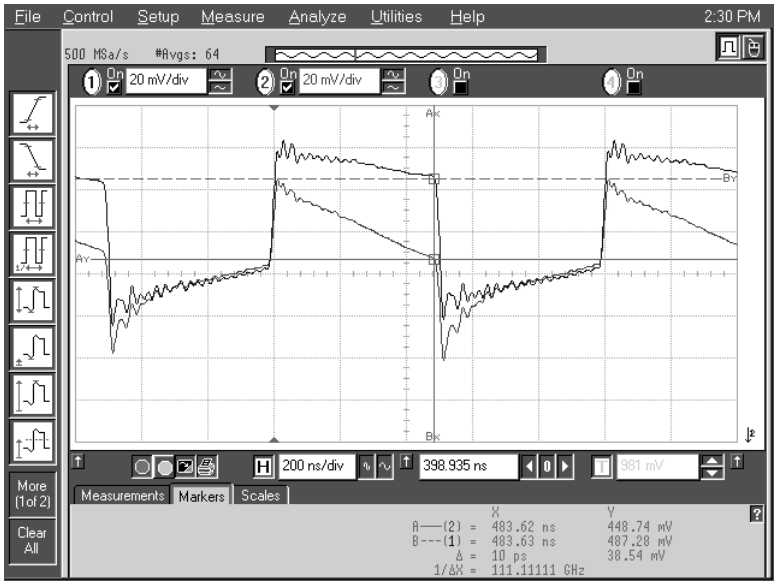

Figure 4.17 300nA input current response at 1MHz clock rate

The next step was to test the circuit's response to a negative current input. A -300nA DC current was applied to the input of the current mirror, and gave the result shown in Figure 4.18. The application of a -300nA test current to the current mirror input caused a differential voltage output change of only 24.9mV, which corresponds to a transimpedance gain of under 90kΩ.

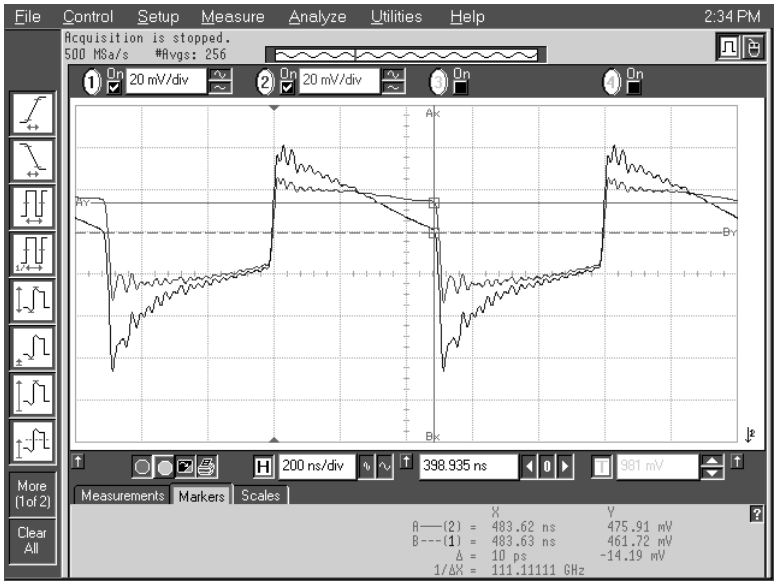

Figure 4.18 -300nA input current response at 1MHz clock rate

The overall discrepancies in gain can be attributed to multiple sources, including high sensitivity to parasitic capacitances, variation in the higher-impedance single-to-differential current mirror, and an overly ambitious reduction in overall circuit power consumption and drive strength.

Integrator Using Correlated Double Sampling

The correlated double sampling TIA was a complex design that required a 2MHz clock input that was divided down to two out-of-phase 1MHz clocks by a set of on-die flip flops. The 1MHz clocks were then fed into two separate non-overlapping clock generators with clock booster circuits attached to the outputs. The overall clocking scheme was complex and left significant room for errors. It also had the disadvantage of having an integration phase that lasted less than 250ns when a 1MHz

clock was used. As with the resistive TIA design, the correlated double sampling design was attached to the output pins using a set of analog multiplexing switches. Both a standalone version and two copies of the circuit with main amplifiers and modulators were fabricated. No visible response to any input current input could be seen from any of the correlated double sampling designs.

The slow integrator design utilized a special three-phase, 125 kHz clock. The use of this slow clock gave the circuit the advantage of an integrating phase that lasted approximately 15μs. This allowed ample time for small currents to be integrated onto the sampling capacitor before the circuit reset, creating a much cleaner output signal in simulation.

The circuit was tested by sweeping the input current from -90nA to +90nA in 10nA increments. A test script was written to change the current input, wait two seconds and measure the DC output level, increase the input current, and repeat. The script was used to test a sample set of 20 chips. The resulting input current vs. output voltage is shown in Figure 4.19.

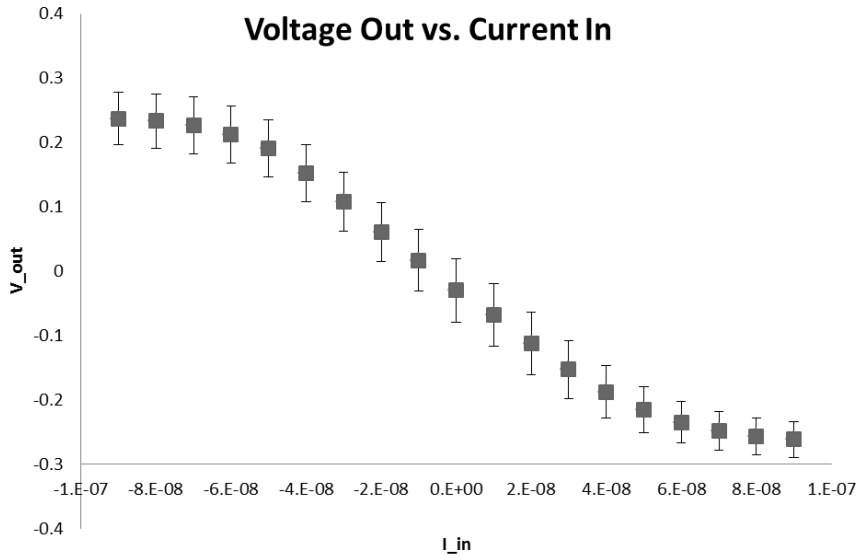

Figure 4.19 Integrator output voltage vs. input current

The circuit appears to have a transimpedance gain of approximately 5MΩ while still operating linearly. As the input current magnitude increases to above 50nA, the circuit's output begins to saturate. This transimpedance gain was a factor of 10 lower

than the designed gain. The circuit was also tested using a 10nA sinusoidal current input, giving the result shown in Figure 4.20.

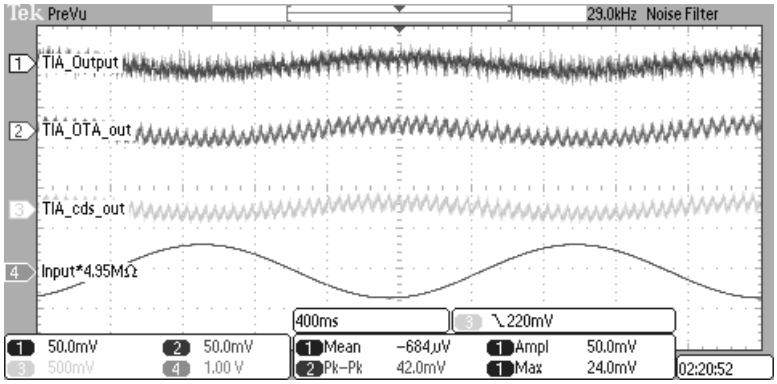

Figure 4.20 Integrator response to a 10nA sinusoidal input current

The circuit operated at a consistent 125 kHz clock rate, and the three internal node voltages appeared to integrate as expected. The output, although somewhat noisy, had the expected track-and-hold operation pattern. With the oscilloscope's noise filter bandwidth decreased, the circuit output and internal node voltages appeared as clean sinusoidal voltages, as seen in Figure 4.21.

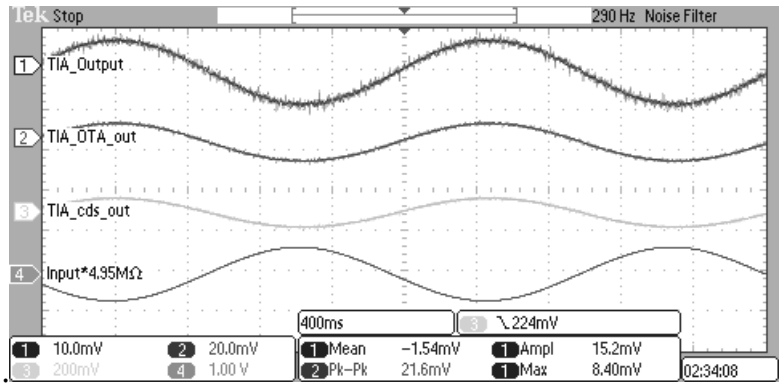

Figure 4.21 Filtered circuit response to a 10nA sinusoidal input current

An additional measurement with no noise filter was taken to show the detail of the integrating operation of the internal node voltages. This measurement is shown in Figure 4.20.

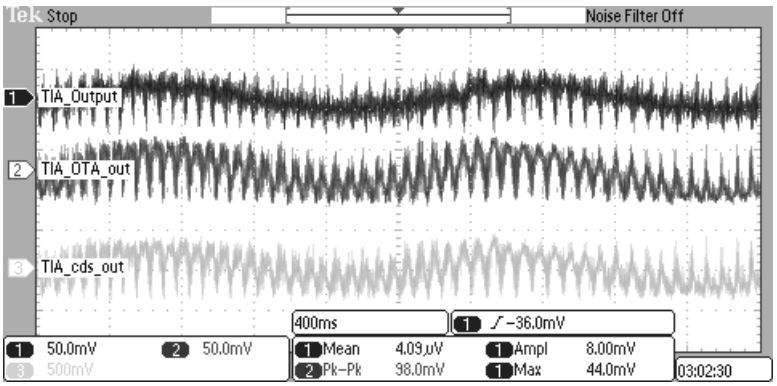

Figure 4.22 Circuit response showing detailed integration phases

The integrator operated as expected, with the exception of the reduced transimpedance gain. After further investigation and simulation, it was discovered that parasitic capacitances on the internal nodes could have an effect on the gain of the circuit, by offsetting the expected ratio of the two capacitors. The circuit was designed with the intention of having minimal capacitance on the internal node routing. At the time of the final layout before fabrication, it was decided that probing the internal node voltages using on chip voltage buffers would be beneficial to the overall debugging of the circuit design. One potential method to solve this issue would be to simply build the circuit without the internal node voltage being probed. This could solve the issue, but runs the risk of having no response at the output with no debugging tools available. Another solution would be to increase the size of the internal capacitances as well as the overall current consumed by the amplifier, but this would be compromising the small size and power consumption of the overall circuit.

Chapter 5

Conclusions, Discussion and Suggestions

Conclusions

We have developed an electrochemical sensor for nitric oxide that is based on multi-layers of nickel (II) phthalocyaninetetrasulfonate and a polyamidoamine dendrimer assembled on the surface of a carbon-fiber microelectrode. This sensor responds to nitric oxide at a working potential of 800 mV with a sensitivity of 5.54 pA μM^{-} 1 which, however, depends on the dendrimer layer position deposited on the microelectrode. The limit of detection is as low as 5.5 μM at a signal-to-noise ratio of 3. The electrode exhibits good selectivity for nitric oxide over common interferents including dopamine, nitrite, hydrogen peroxide, norepinephrine, epinephrine and ascorbic acid. A NO sensor based on alternate NiTsPc and PAMAM layers assembled on a carbon fiber microelectrode was developed. The CF-(PAMAM/NiTsPc) sensor showed the best performance for NO detection when compared to another modified electrodes. For example, this sensor type is able to detect NO in aqueous solutions in the presence of high concentrations of interferents such as $NO2^{-}$, H2O2, DA, UA, NEp, Ep and AA. This study thus shows the potential of new sensor composed by phthalocyanine and dendrimer molecule for quantification of NO in vitro and in vivo. However, for practical deployment of the sensor, additional work necessary to explore the properties of the CF-(PAMAM/NiTsPc) sensor in real biological samples (e.g. cell culture media and biological fluids among others). Besides the need for detailed investigation of the long-term stability of the sensor and possible biofouling of the sensor components, biocompatibility also needs to be tested. Additionally, the sensitivity needs to be further improved for very low concentrations of NO in biological sources. Furthermore, the study also introduces the use of EIS not only for characterizing sensor performances and understanding the mechanisms behind these performances, but also for quantification of NO.

As a messenger molecule, NO plays important roles in living system. It is highly relevant to develop a fast and sensitive detectionmethod for NO in biological samples

and organisms. Of the known techniques, nanotechnology presents a bright prospect for the development of NO sensors. This review has mainly addressed recent advances of electrochemical NO sensors based on carbon, metal, semiconductor and hybrid nanoparticles. Throughout this review these nanoparticles are attractive materials for NO sensors applications, because of their several advantages : (i) The nano-scaled size (1–100 nm) and correspondingly large surface-to-volume ratio could generate a roughened conductive-high-surface area interface, which can increases the surface absorption capability and enables the sensitive detection of NO. (ii) The excellent conductivity and catalytic activity speed up the rate of electron transfer and decrease the anodic or cathodic over potential of NO. (iii) Chemically tailoring and functionalization for nanoparticles with macrocyclic molecular, polymer, biomaterial or other nanomaterial coatings reveal that diverse NO sensors could be tailored on kinds of the electrode surface using such functional nanoparticles in order to improve the analytical performance of NO detection.

Throughout the evolution of the transimpedance amplifier designs, several trends have become apparent. Charge injection must be carefully monitored throughout the design of a transimpedance amplifier. Since the overall purpose of a TIA is to measure current, and one of the most noise-effective methods of doing this is to integrate the current on a capacitor, charge injection can significantly decrease the precision of a transimpedance amplifier.

A second trend that has become apparent is that circuits amplify small currents significantly better at lower clock rates. It is likely that this observation is due to the simple fact that operating at a slower clock rate allows more charge to accumulate, creating a voltage that is larger and an overall lower amount of noise due to switching. An additional important parameter that has been observed throughout the course of these designs is the linearity of capacitors. If a circuit is being used to amplify a bi-directional current input (both positive and negative magnitude), it is extremely important that the integration capacitors are linear in both possible voltage directions. In the case of national’s poly-poly capacitors, it was discovered that the charging characteristics weren’t symmetrical. Placing two capacitors in opposite orientations in parallel in place of the original capacitor significantly helped improve the charging characteristics of the overall circuit. Finally, low power consumption and high

impedance nodes must be carefully balanced. Increasing overall impedance from the positive to negative supply rails can significantly decrease power consumption, but it can also significantly increase the effects of process variation on theoverall node voltages. Feedback and voltage stabilization techniques should always be considered when designing low-power circuits.

Discussion

The measurements of NO have been proven to face great challenges because of its low concentration, complex coexistence and high reactivity in vivo. Although the unique properties of nanoparticles have offered many advantages for their applications in NO sensors, further efforts should be made focusing on: (i) the development of functional nanoparticles that are soluble and long-term stable in different buffered saline solutions, and amenable to limited non-specific binding to fabricate NO analysis systems with better sensitivities and selectivity; (ii) the miniaturization of the nanoparticles ensembles with the ultimate goal of using a single functionalized nanoparticle, such as nanotube or nanowire, for the witnessed and in vivo sensing of NO; (iii) the extending application of semiconductor nanoparticles or quantum dots (QDs) nanocrystals for developing ultra-sensitive, multiplexed NO sensor; (iv) the combination of different analytical techniques, such as electrochemistry, spectroscopy and chromatography, based on different type of nanoparticles or their functionalized particles. In conclusion, the application of nanoparticles and the nanoscale dimension of the active sensing elements in the fabrication of NO sensor will require continued interdisciplinary efforts of researchers worldwide. Look forward to new generations of miniaturized NO sensing devices with high sensitivity and excellent selectivity.

The performance parameters of the final TIA design were compared with a few state of the art designs, as shown in Table 5.1. The overall power consumption and input referred noise currents were significantly lower than other published integrator designs. When comparing power consumption parameters, it must be considered that the design presented in this thesis didn’t include features such as variable gain or automatic gain control, and the overall bandwidth of some of the compared circuits may have been significantly higher than the bandwidth of the presented design.

Table 5.1 Transimpedance amplifier performance comparison

	Simulation*	**Sharma et al.**	**Ferrari et al.**	**Razavi et al.**	**Salvia et al.**	**Zand et al.**	**Balasubramanian et al.**	**Tang et al.**
Power	8.06µW@ 0.9V	400µW	45mW @3V	30mW @3V	436µW@ 1.8V	30mW @3V	90µW @1.8V	3.2 mW
Gain	50MΩ	>25MΩ	60MΩ	8.7kΩ	56MΩ	33kΩ	150KΩ - 550KΩ	88MΩ
Spot Noise	981aA/ √Hz @ 1kHz	88fA/ √Hz @ 1.6MΩ	4fA/ √Hz	n/a	65fA/ √Hz	n/a	n/a	25fA/ √Hz
Avg. Noise	1.08pA/√Hz	n/a	n/a	4.5pA/√ Hz	n/a	6.8pA/ √Hz	1.6pA/√Hz	n/a

Suggestions

The future work should be put toward refining the performance of the individual circuits as well as improving the overall integration of the electronics system. With these improvements, a novel, high-performance biosensor system can be achieved. The hardware must be redesigned to provide for an even higher resolution while allowing the user to select the voltage sweep range and scan rate. Increasing the number of data points above the current 50 points would provide for a smoother curve and result in fewer noise inflections. This increase in data points could be accomplished by using a 10 or 12 bit DAC and a digitally controlled attenuator, as well as a few software changes to accommodate the new parts. These changes would need to be implemented with the device size in mind as the hardware used to construct the circuit should be minimized; the next prototype should approach the size of other biosensors currently on the market. In addition, the selection of initial and peak voltages as well as the scan rate would need

to be reconfigured. Implementing these user controls into the software would result in fewer external switches, again minimizing device size. The electrode system needs to be refined so that a screen printing process can be used such that all three electrodes could reside on a single disposable strip of polyester film. The electrode fabrication method would need to be configured alongside the chemistry process because the current method of NO isolation would not be feasible for mass production. And third, a new software interface as well as a data handling system needs to be created. An algorithm to calculate the area of the peaks of the resulting cyclic voltammograms in real time is required.

Besides the need for detailed investigation of the long-term stability of the sensor and possible bio fouling of the sensor components, biocompatibility also needs to be tested. Additionally, the sensitivity needs to be further improved for very low concentrations of NO in biological sources. Furthermore, the study also introduces the use of EIS not only for characterizing sensor performances and understanding the mechanisms behind these performances, but also for quantification of NO.

References

Alencar, W. S., Crespilho, F. N., Santos, M. R. M. C., Zucolotto, V., Oliveira, O. N., & Silva, W. C. (2007). Influence of Film Architecture on the Charge-Transfer Reactions of Metallophthalocyanine Layer-by-Layer Films. *The Journal of Physical Chemistry C, 111*(34), 12817-12821. DOI:10.1021/jp070695r

Allen, B. W., Liu, J., & Piantadosi, C. A. (2005) Electrochemical detection of nitric oxide in biological fluids. *Vol. 396. Methods in Enzymology* (pp. 68-77).

Amatore, C., Arbault, S., Guille, M., & Lemaître, F. (2008). Electrochemical monitoring of single cell secretion: Vesicular exocytosis and oxidative stress. *Chemical Reviews, 108*(7), 2585-2621. DOI:10.1021/cr068062g

Asahi, M., Fujii, J., Suzuki, K., Seo, H. G., Kuzuya, T., Hori, M., . . . Taniguchi, N. (1995). Inactivation of glutathione peroxidase by nitric oxide: Implication for cytotoxicity. *Journal of Biological Chemistry, 270*(36), 21035-21039. Retrieved from http://www.scopus.com/inward/record.url?eid=2-s2.0-0029099103&partnerID=40&md5=a580df10e9d97206948daaa2b08f8670

Balasubramanian, V., Ruedi, P. F., Temiz, Y., Ferretti, A., Guiducci, C., & Enz, C. C. (2013). A 0.18 μ m biosensor front-end based on 1/f noise, distortion cancelation and chopper stabilization techniques. *IEEE Transactions on Biomedical Circuits and Systems, 7*(5), 660-673. DOI:10.1109/TBCAS.2012.2234121

Becker, K., Gui, M., & Schirmer, R. H. (1995). Inhibition of human glutathione reductase by S-nitrosoglutathione. *European Journal of Biochemistry, 234*(2), 472-478. Retrieved from http://www.scopus.com/inward/record.url?eid=2-s2.0-0028881049&partnerID=40&md5=66fa93be344f47a03ee60ed0c7d95a69

Beckman, J. S., Beckman, T. W.3, Chen, J., Marshall, P. A., & Freeman, B. A. (1990). Apparent hydroxyl radical production by peroxynitrite: Implications for endothelial injury from nitric oxide and superoxide. *Proceedings of the National Academy of Sciences of the United States of America, 87*(4), 1620-1624. Retrieved from http://www.scopus.com/inward/record.url?eid=2-s2.0-0025189864&partnerID=40&md5=49484317122d5d78980413fdbc6376ca

Beckman, J. S., & Crapo, J. D. (1997). The Role of Nitric Oxide in Limiting Gene Transfer: Parallels to Viral Host Defenses. *American Journal of Respiratory Cell and Molecular Biology, 16*(5), 495-496. Retrieved from http://www.scopus.com/inward/record.url?eid=2-s2.0-0031135504&partnerID=40&md5=9aff2a88b39fe5cb52f875587c80165e

Biesaga, M., Pyrzyńska, K., & Trojanowicz, M. (2000). Porphyrins in analytical chemistry. A review. *Talanta, 51*(2), 209-224. DOI:10.1016/S0039-9140(99)00291-X

Böger, G. I., Rudolph, T. K., Maas, R., Schwedhelm, E., Dumbadze, E., Bierend, A., . . . Böger, R. H. (2007). Asymmetric Dimethylarginine Determines the Improvement of Endothelium-Dependent Vasodilation by Simvastatin: Effect of Combination With Oral L-Arginine. *Journal of the American College of Cardiology, 49*(23), 2274-2282. DOI:http://dx.doi.org/10.1016/j.jacc.2007.02.051

Borgmann, S. (2009). Electrochemical quantification of reactive oxygen and nitrogen: Challenges and opportunities. *Analytical and Bioanalytical Chemistry, 394*(1), 95-105. DOI:10.1007/s00216-009-2692-1

Bottino, E., Massobrio, P., Martinoia, S., Pruzzo, G., & Valle, M. (2009). Low-noise low-power CMOS preamplifier for multisite extracellular neuronal recordings. *Microelectronics Journal, 40*(12), 1779-1787. DOI:http://dx.doi.org/10.1016/j.mejo.2009.10.003

Bratt, J. M., Zeki, A. A., Last, J. A., & Kenyon, N. J. (2011). Competitive metabolism of L-arginine: arginase as a therapeutic target in asthma(). *Journal of Biomedical Research, 25*(5), 299-308. DOI:10.1016/S1674-8301(11)60041-9

Buerk, D. G. (2001) Can we model nitric oxide biotransport? A survey of mathematical models for a simple diatomic molecule with surprisingly complex biological activities. *Vol. 3. Annual Review of Biomedical Engineering* (pp. 109-143).

Cancino, J., Borgmann, S., Machado, S. S., Zucolotto, V., Schuhmann, W., & Masa, J. (2015). Electrochemical sensor for nitric oxide using layered films composed of a polycationic dendrimer and nickel(II)

phthalocyaninetetrasulfonate deposited on a carbon fiber electrode. *Microchimica Acta, 182*(5-6), 1079-1087. DOI:10.1007/s00604-014-1425-0

Chen, K., Pittman, R. N., & Popel, A. S. (2008). Nitric Oxide in the Vasculature: Where Does It Come From and Where Does It Go? A Quantitative Perspective. *Antioxidants & Redox Signaling, 10*(7), 1185-1198. DOI:10.1089/ars.2007.1959

Chiu, J.-J., & Chien, S. (2011). Effects of Disturbed Flow on Vascular Endothelium: Pathophysiological Basis and Clinical Perspectives. *Physiological reviews, 91*(1), 10.1152/physrev.00047.02009. DOI:10.1152/physrev.00047.2009

Davies, M. G., Fulton, G. J., & Hagen, P. O. (1995). Clinical biology of nitric oxide. *British Journal of Surgery, 82*(12), 1598-1610. DOI:10.1002/bjs.1800821206

Denninger, J. W., & Marletta, M. A. (1999). Guanylate cyclase and the ·NO/cGMP signaling pathway. *Biochimica et Biophysica Acta (BBA) - Bioenergetics, 1411*(2–3), 334-350. DOI:http://dx.doi.org/10.1016/S0005-2728(99)00024-9

Durand, M. J., & Gutterman, D. D. (2013). Diversity in Mechanisms of Endothelium-Dependent Vasodilation in Health and Disease. *Microcirculation (New York, N.Y. : 1994), 20*(3), 239-247. DOI:10.1111/micc.12040

Ferrari, G., Gozzini, F., & Sampietro, M. (2006). Transimpedance amplifiers for extremely high sensitivity impedance measurements on nanodevices *Analog Circuit Design: High-speed Clock and Data Recovery, High-performance Amplifiers, Power Management* (pp. 193-207).

Goldstein, I. M., Ostwald, P., & Roth, S. (1996). Nitric Oxide: A Review of Its Role in Retinal Function and Disease. *Vision Research, 36*(18), 2979-2994. DOI:http://dx.doi.org/10.1016/0042-6989(96)00017-X

Hardy, T. A., & May, J. M. (2002). Coordinate regulation of L-arginine uptake and nitric oxide synthase activity in cultured endothelial cells. *Free Radical Biology and Medicine, 32*(2), 122-131. DOI:10.1016/s0891-5849(01)00781-x

Hengstenberg, A. (2001). Spatially resolved detection of neurotransmitter secretion from individual cells by means of scanning electrochemical microscopy. *Angewandte Chemie - International Edition, 40*(5), 905-908. DOI:10.1002/1521-3773(20010302)40:5<905::AID-ANIE905>3.0.CO;2-#

Hoshino, M., Laverman, L., & Ford, P. C. (1999). Nitric oxide complexes of metalloporphyrins: An overview of some mechanistic studies. *Coordination Chemistry Reviews, 187*(1), 75-102. Retrieved from http://www.scopus.com/inward/record.url?eid=2-s2.0-0033420652&partnerID=40&md5=155b261df20c3ea3a86a2b3da4bea964

Hsiao, S.-H., & Tsai, L.-J. (2008). A Neurovascular Transmission Model for Acupuncture-induced Nitric Oxide. *Journal of Acupuncture and Meridian Studies, 1*(1), 42-50. DOI:http://dx.doi.org/10.1016/S2005-2901(09)60006-6

Jin, J., Miwa, T., Mao, L., Tu, H., & Jin, L. (1999). Determination of nitric oxide with ultramicrosensors based on electropolymerized films of metal tetraaminophthalocyanines. *Talanta, 48*(5), 1005-1011. DOI:10.1016/S0039-9140(98)00308-7

Johnson, C. R., & Shepherd, R. E. (1983). The pKa of pyraziniumpentacyanoruthenate(II), (CN)5Ru(pzH)2. *Inorganic Chemistry, 22*(7), 1117-1123. DOI:10.1021/ic00149a023

Kelm, M. (1999). Nitric oxide metabolism and breakdown. *Biochimica et Biophysica Acta (BBA) - Bioenergetics, 1411*(2–3), 273-289. DOI:http://dx.doi.org/10.1016/S0005-2728(99)00020-1

Kolluru, G. K., Bir, S. C., & Kevil, C. G. (2012). Endothelial dysfunction and diabetes: Effects on angiogenesis, vascular remodeling, and wound healing. *International Journal of Vascular Medicine, 2012*. DOI:10.1155/2012/918267

Kuchan, M. J., & Frangos, J. A. (1994). Role of calcium and calmodulin in flow-induced nitric oxide production in endothelial cells. *American Journal of Physiology - Cell Physiology, 266*(3 35-3), C628-C636. Retrieved from http://www.scopus.com/inward/record.url?eid=2-s2.0-0028329851&partnerID=40&md5=052093e1dfe52fd75e37e9b28d803e63

Levy, A. S., Chung, J. C. S., Kroetsch, J. T., & Rush, J. W. E. (2009). Nitric oxide and coronary vascular endothelium adaptations in hypertension. *Vascular Health and Risk Management, 5*, 1075-1087. Retrieved from http://www.ncbi.nlm.nih.gov/pmc/articles/PMC2801631/

Loscalzo, J. (2000). What we know and don't know about L-arginine and NO. *Circulation, 101*(18), 2126-2129. Retrieved from

http://www.scopus.com/inward/record.url?eid=2-s2.0-0034624994&partnerID=40&md5=75cfd88c07d7cbfe0697a54a7f9a3a84

Malinski, T., & Taha, Z. (1992). Nitric oxide release from a single cell measured in situ by a porphyrinic-based microsensor. *Nature, 358*(6388), 676-678. Retrieved from http://www.scopus.com/inward/record.url?eid=2-s2.0-0026737394&partnerID=40&md5=2e886729df206457542c547dd2ab7a6a

Mayer, B., Schrammel, A., Klatt, P., Koesling, D., & Schmidt, K. (1995). Peroxynitrite-induced accumulation of cyclic GMP in endothelial cells and stimulation of purified soluble guanylyl cyclase: Dependence on glutathione and possible role of S-nitrosation. *Journal of Biological Chemistry, 270*(29), 17355-17360. Retrieved from http://www.scopus.com/inward/record.url?eid=2-s2.0-0029116612&partnerID=40&md5=d16996c087e844615855fce2fcb7d6b1

Noronha-Dutra, A. A., Epperlein, M. M., & Woolf, N. (1993). Reaction of nitric oxide with hydrogen peroxide to produce potentially cytotoxic singlet oxygen as a model for nitric oxide-mediated killing. *FEBS Letters, 321*(1), 59-62. DOI:10.1016/0014-5793(93)80621-Z

Oni, J., Pailleret, A., Isik, S., Diab, N., Radtke, I., Blöchl, A., . . . Schuhmann, W. (2004). Functionalised electrode array for the detection of nitric oxide released by endothelial cells using different NO-sensing chemistries. *Analytical and Bioanalytical Chemistry, 378*(6), 1594-1600. DOI:10.1007/s00216-004-2512-6

Pacher, P., Beckman, J. S., & Liaudet, L. (2007). Nitric Oxide and Peroxynitrite in Health and Disease. *Physiological reviews, 87*(1), 315-424. DOI:10.1152/physrev.00029.2006

Palmer, R. M. J., Bridge, L., Foxwell, N. A., & Moncada, S. (1992). The role of nitric oxide in endothelial cell damage and its inhibition by glucocorticoids. *British Journal of Pharmacology, 105*(1), 11-12. Retrieved from http://www.scopus.com/inward/record.url?eid=2-s2.0-0026586461&partnerID=40&md5=91d8c25d97b1fa9d0dbae209476f9b00

Patel, R. P., McAndrew, J., Sellak, H., White, C. R., Jo, H., Freeman, B. A., & Darley-Usmar, V. M. (1999). Biological aspects of reactive nitrogen species.

Biochimica et Biophysica Acta (BBA) - Bioenergetics, 1411(2–3), 385-400. DOI:http://dx.doi.org/10.1016/S0005-2728(99)00028-6

Pawloski, J. R., Hess, D. T., & Stamler, J. S. (2001). Export by red blood cells of nitric oxide bioactivity. *Nature, 409*(6820), 622-626. Retrieved from http://dx.doi.org/10.1038/35054560

Pezzuto, L., & Bohlen, H. G. (2008). Extracellular arginine rapidly dilates in vivo intestinal arteries and arterioles through a nitric oxide mechanism. *Microcirculation (New York, N.Y. : 1994), 15*(2), 123-135. DOI:10.1080/10739680701447415

Qi, P., Vermesh, O., Grecu, M., Javey, A., Wang, Q., Dai, H., . . . Cho, K. J. (2003). Toward large arrays of multiplex functionalized carbon nanotube sensors for highly sensitive and selective molecular detection. *Nano Letters, 3*(3), 347-351. DOI:10.1021/nl034010k

Riera, J. J., Schousboe, A., Waagepetersen, H. S., Howarth, C., & Hyder, F. (2008). The micro-architecture of the cerebral cortex: Functional neuroimaging models and metabolism. *NeuroImage, 40*(4), 1436-1459. DOI:10.1016/j.neuroimage.2007.12.051

Roveda Jr, A. C., Papa, T. B. R., Castellano, E. E., & Franco, D. W. (2014). PAMAM dendrimers functionalized with ruthenium nitrosyl as nitric oxide carriers Metallodendrimers Special Issue. *Inorganica Chimica Acta, 409*(PART A), 147-155. DOI:10.1016/j.ica.2013.07.009

Russell, K. S., Haynes, M. P., Caulin-Glaser, T., Rosneck, J., Sessa, W. C., & Bender, J. R. (2000). Estrogen Stimulates Heat Shock Protein 90 Binding to Endothelial Nitric Oxide Synthase in Human Vascular Endothelial Cells: EFFECTS ON CALCIUM SENSITIVITY AND NO RELEASE. *Journal of Biological Chemistry, 275*(7), 5026-5030. DOI:10.1074/jbc.275.7.5026

Sato, H., Sagami, I., Daff, S., & Shimizu, T. (1998). Autoxidation rates of neuronal nitric oxide synthase: Effects of the substrates, inhibitors, and modulators. *Biochemical and Biophysical Research Communications, 253*(3), 845-849. DOI:10.1006/bbrc.1998.9851

Schmidt, K., Kolesnik, B., Gorren, A. C. F., Werner, E. R., & Mayer, B. (2014). Cell type-specific recycling of tetrahydrobiopterin by dihydrofolate reductase

explains differential effects of 7,8-dihydrobiopterin on endothelial nitric oxide synthase uncoupling. *Biochemical Pharmacology, 90*(3), 246-253. DOI:10.1016/j.bcp.2014.05.010

Sharma, A., Zaman, M. F., & Ayazi, F. (2007). A 104-dB dynamic range transimpedance-based CMOS ASIC for tuning fork microgyroscopes. *IEEE Journal of Solid-State Circuits, 42*(8), 1790-1802. DOI:10.1109/JSSC.2007.900282

Souto, J., de Saja, J. A., Gobernado-Mitre, M. I., Rodriguez, M. L., & Aroca, R. (1993). NOx gas detection with Langmuir-Blodgett monolayers of tetra-tert-butyl phthalocyanine complexes. *Sensors and Actuators: B. Chemical, 16*(1-3), 306-311. DOI:10.1016/0925-4005(93)85200-T

Stasko, N. A., & Schoenfisch, M. H. (2006). Dendrimers as a scaffold for nitric oxide release. *Journal of the American Chemical Society, 128*(25), 8265-8271. DOI:10.1021/ja060875z

Stuehr, D. J. (1999). Mammalian nitric oxide synthases. *Biochimica et Biophysica Acta (BBA) - Bioenergetics, 1411*(2–3), 217-230. DOI:http://dx.doi.org/10.1016/S0005-2728(99)00016-X

Tang, Y., Zhang, Y., Fedder, G. K., & Carley, L. R. (2012). *An ultra-low noise Switched Capacitor Transimpedance Amplifier for parallel Scanning Tunneling Microscopy.* Paper presented at the Proceedings of IEEE Sensors.

Tengan, C. H., Rodrigues, G. S., & Godinho, R. O. (2012). Nitric oxide in skeletal muscle: Role on mitochondrial biogenesis and function. *International Journal of Molecular Sciences, 13*(12), 17160-17184. DOI:10.3390/ijms131217160

Tripathi, V., & Krishna, A. (2008). Changes in nitric oxide (NO) synthase isoforms and NO in the ovary of Heteropneustes fossilis (Bloch.) during the reproductive cycle. *Journal of Endocrinology, 199*(2), 307-316. DOI:10.1677/joe-07-0509

Tuteja, N., Chandra, M., Tuteja, R., & Misra, M. K. (2004). Nitric Oxide as a Unique Bioactive Signaling Messenger in Physiology and Pathophysiology. *Journal of Biomedicine and Biotechnology, 2004*(4), 227-237. DOI:10.1155/S1110724304402034

Uttara, B., Singh, A. V., Zamboni, P., & Mahajan, R. T. (2009). Oxidative Stress and Neurodegenerative Diseases: A Review of Upstream and Downstream Antioxidant Therapeutic Options. *Current Neuropharmacology, 7*(1), 65-74. DOI:10.2174/157015909787602823

Whit Walker, M., Kinter, M. T., Roberts, R. J., & Spitz, D. R. (1995). Nitric oxide-induced cytotoxicity: Involvement of cellular resistance to oxidative stress and the role of glutathione in protection. *Pediatric Research, 37*(1), 41-49. Retrieved from http://www.scopus.com/inward/record.url?eid=2-s2.0-0028894060&partnerID=40&md5=f832330ae65581adb05f5e1dc2a43d1b

Xu, C., Lemon, W., & Liu, C. (2002). Design and fabrication of a high-density metal microelectrode array for neural recording. *Sensors and Actuators, A: Physical, 96*(1), 78-85. DOI:10.1016/S0924-4247(01)00766-X

Zand, B., Phang, K., & Johns, D. A. (2001). *A transimpedance amplifier with DC-coupled differential photodiode current sensing for wireless optical communications.* Paper presented at the Proceedings of the Custom Integrated Circuits Conference.

Zhang, X., Cardosa, L., Broderick, M., Fein, H., & Lin, J. (2000). An integrated nitric oxide sensor based on carbon fiber coated with selective membranes. *Electroanalysis, 12*(14), 1113-1117. DOI:10.1002/1521-4109(200010)12:14<1113::AID-ELAN1113>3.0.CO;2-U

Zhang, X., Kislyak, Y., Lin, J., Dickson, A., Cardosa, L., Broderick, M., & Fein, H. (2002). Nanometer size electrode for nitric oxide and S-nitrosothiols measurement. *Electrochemistry Communications, 4*(1), 11-16. DOI:10.1016/S1388-2481(01)00265-X

Zhang, X., Zhang, W., Zhou, X., & Ogorevc, B. (1996). Fabrication, Characterization, and Potential Application of Carbon Fiber Cone Nanometer-Size Electrodes. *Analytical Chemistry, 68*(19), 3338-3343. Retrieved from http://www.scopus.com/inward/record.url?eid=2-s2.0-0000561274&partnerID=40&md5=bea4815f824d270edc183e2fe50568a4

Zheng, D., Hu, C., Peng, Y., Yue, W., & Hu, S. (2008). Noncovalently functionalized water-soluble multiwall-nanotubes through azocarmine B and their application

in nitric oxide sensor. *Electrochemistry Communications, 10*(1), 90-94. DOI:10.1016/j.elecom.2007.10.027

Appendices

Appendix A

Source Code of Experiments for Biosensor Circuit

Source Code for Inverter Sizing

```
simulator( 'spectre )
design( "/home/rselby/simulation/inv_test_ocean/spectre/schematic/netlist/netlist")
resultsDir( "/home/rselby/simulation/inv_test_ocean/spectre/schematic" )
modelFile(
'("/space/analog_design_DB/national_semi_cadence/NSCmodels/spectre_current/typ_cmos9t5v/cmos9
t5v_definition.scs" "")
'("/space/analog_design_DB/national_semi_cadence/NSCmodels/spectre_current/typ_cmos9t5v/cmos9
t5v_corner.scs" "")
)
analysis('dc ?saveOppoint t ?param "pWidth" ?start "220n"
?stop "50u" )
desVar( "pLength" 250n )
desVar( "pWidth" 1u )
envOption(
'analysisOrder list("dc" "ac")
)
temp( 27 )
run()
selectResult( 'dc )
plot(getData("/diode_connected_out") )
\4\5\0mV_crossing = cross(v("/diode_connected_out" ?result "dc-dc") 0.45 1 "either" nil nil)
                        plot( \4\5\0mV_crossing ?expr '( "450mV_crossing" ) )
```

Source Code for OTA Optimization

```
simulator( 'spectre )
design( "inv_opamp_testlib_willy" "inv_opamp_fully_differential_ocean" "schematic")
cellview = dbOpenCellViewByType("inv_opamp_testlib_willy"
"inv_opamp_fully_differential_ocean" "schematic" "" "r")
modelFile(
'("/space/analog_design_DB/national_semi_cadence/NSCmodels/spectre_current/typ_cmos9t5v/cmos9
t5v_definition.scs" "")
```

```
'("/space/analog_design_DB/national_semi_cadence/NSCmodels/spectre_current/typ_cmos9t5v/cmos9
t5v_corner.scs" "")
)
;;Functions needed to change W/L in devices
load("/home/willyw/OceanScripts/CCSinvokedCdfCallbacks.il")
load("/home/willyw/OceanScripts/changeCDF.il")
;load("/home/willyw/OceanSizingData/InverterSizingData/Final/700mV_vdd/0.5vdd/0.5vdd_1.5um_le
ngth.csv")
load("/home/willyw/OceanTest/0.5vdd_1.5um_length.csv.pp.pp")
load("/home/willyw/OceanTest/1.5uTail700mV.csv.pp.pp")
xcorner_full_l = list("typ,27")
supply = 0.7;
analysis('ac ?start "1" ?stop "10G" )
analysis('dc ?saveOppoint t )
analysis('tran ?stop "2m" ?errpreset "conservative" )
desVar( "amp" 1u )
;desVar( "compCap" 0 )
desVar( "f" 1k )
desVar( "load" 1p )
desVar( "supply" 0.7)
desVar( "vinDC" 350m )
envOption(
'analysisOrder list("dc" "tran" "ac")
)
save( 'i "/vSupply/MINUS" )
temp( 27 )
foreach(isize xsize_l
parsedi = parseString(isize ",")
printf("%s" isize)
in_nWidth = evalstring(nthelem(1 parsedi))
in_nLength = evalstring(nthelem(2 parsedi))
in_pWidth = evalstring(nthelem(3 parsedi))
in_pLength = evalstring(nthelem(4 parsedi))
foreach(xsize xsize_l
;nWidth,nLength,pWidth,pLength,Power,Current
parsed = parseString(xsize ",")
nWidth = evalstring(nthelem(1 parsed))
nLength = evalstring(nthelem(2 parsed))
```

```
pWidth = evalstring(nthelem(3 parsed))
pLength = evalstring(nthelem(4 parsed))
foreach(tsize tsize_l
parsed2 = parseString(tsize ",")
nTailWidth = evalstring(nthelem(1 parsed2))
nTailLength = evalstring(nthelem(2 parsed2))
pTailWidth = evalstring(nthelem(3 parsed2))
pTailLength = evalstring(nthelem(4 parsed2))
if(nWidth > 0 then
;Create variables to hold length and width data for FETs
sprintf(neg_input_p_w "%g" in_pWidth)
sprintf(neg_input_p_l "%g" in_pLength)
sprintf(neg_input_n_w "%g" in_nWidth)
sprintf(neg_input_n_l "%g" in_nLength)
sprintf(pos_input_p_w "%g" in_pWidth)
sprintf(pos_input_p_l "%g" in_pLength)
sprintf(pos_input_n_w "%g" in_nWidth)
sprintf(pos_input_n_l "%g" in_nLength)
sprintf(neg_load_p_w "%g" pWidth)
sprintf(neg_load_p_l "%g" pLength)
sprintf(neg_load_n_w "%g" nWidth)
sprintf(neg_load_n_l "%g" nLength)
sprintf(pos_load_n_w "%g" nWidth)
sprintf(pos_load_n_l "%g" nLength)
sprintf(pos_load_p_w "%g" pWidth)
sprintf(pos_load_p_l "%g" pLength)
sprintf(tail_p_w "%g" pTailWidth)
sprintf(tail_p_l "%g" pTailLength)
sprintf(tail_n_w "%g" nTailWidth)
sprintf(tail_n_l "%g" nTailLength)
;Change lengths and widths.
changeCDF(cellview "neg_input_p" "w" neg_input_p_w)
changeCDF(cellview "neg_input_p" "l" neg_input_p_l)
changeCDF(cellview "neg_input_n" "w" neg_input_n_w)
changeCDF(cellview "neg_input_n" "l" neg_input_n_l)
changeCDF(cellview "pos_input_p" "w" pos_input_p_w)
changeCDF(cellview "pos_input_p" "l" pos_input_p_l)
changeCDF(cellview "pos_input_n" "w" pos_input_n_w)
```

```
changeCDF(cellview "pos_input_n" "l" neg_input_n_l)
changeCDF(cellview "neg_load_p" "w" neg_load_p_w)
changeCDF(cellview "neg_load_p" "l" neg_load_p_l)
changeCDF(cellview "neg_load_n" "w" neg_load_n_w)
changeCDF(cellview "neg_load_n" "l" neg_load_n_l)
changeCDF(cellview "pos_load_p" "w" pos_load_p_w)
changeCDF(cellview "pos_load_p" "l" pos_load_p_l)
changeCDF(cellview "pos_load_n" "w" pos_load_n_w)
changeCDF(cellview "pos_load_n" "l" neg_load_n_l)
changeCDF(cellview "neg_load_cross_p" "w" neg_load_p_w)
changeCDF(cellview "neg_load_cross_p" "l" neg_load_p_l)
changeCDF(cellview "neg_load_cross_n" "w" neg_load_n_w)
changeCDF(cellview "neg_load_cross_n" "l" neg_load_n_l)
changeCDF(cellview "pos_load_cross_p" "w" pos_load_p_w)
changeCDF(cellview "pos_load_cross_p" "l" pos_load_p_l)
changeCDF(cellview "pos_load_cross_n" "w" pos_load_n_w)
changeCDF(cellview "pos_load_cross_n" "l" neg_load_n_l)
changeCDF(cellview "p_tail" "w" tail_p_w)
changeCDF(cellview "p_tail" "l" tail_p_l)
changeCDF(cellview "n_tail" "w" tail_n_w)
changeCDF(cellview "n_tail" "l" tail_n_l)
;Invoke callbacks
;CCSinvokeCdfCallbacks( cellview )
;Check and save
schCheck(cellview)
dbSave(cellview)
;Generate netlist
createNetlist(?recreateAll t ?display 'nil)
foreach(xcorner_full xcorner_full_l
parsed = parseString(xcorner_full ",")
xcorner = nthelem(1 parsed)
xtemp = nthelem(2 parsed)
sprintf(path
"/home/willyw/OceanSimdata/Inv_Opamp_char/%g_%g_%g_%g_%g_%g_%g_%g_%g_%g_%g_%g_%g
_%g_%s_%s" in_nWidth in_nLength in_pWidth in_pLength nWidth nLength pWidth pLength
nTailWidth nTailLength pTailWidth pTailLength supply xcorner xtemp)
resultsDir(path)
run()
```

```
printf("PATH=%s\n" path)
)
) ;foreach xcorner
) ;if
) ;foreach size
)
;load("mir_cas_verify_nch_dataOrig.ocn");
```

Source code for extracting data from inverter opamp simulations

```
p1 = outfile("/home/willyw/OceanSimdata/1.5u_700mV_vdd.txt" "w")
output_name_string = "in_nWidth in_nLength in_pWidth in_pLength load_nWidth load_nLength
load_pWidth load_pLength tail_nWidth tail_nLength tail_pWidth tail_pLength current Vout VDD
Power GBW Load FOM"
;fprintf(p1 "Extracted on: %s\n" getCurrentTime())
fprintf(p1 "%s\n" output_name_string)
load("/home/willyw/OceanSimdata/Inv_Opamp_char.txt")
foreach(sim sim_l
parsed = parseString(sim "_")
in_nWidth = nthelem(1 parsed)
in_nLength = nthelem(2 parsed)
in_pWidth = nthelem(3 parsed)
in_pLength = nthelem(4 parsed)
load_nWidth = nthelem(5 parsed)
load_nLength= nthelem(6 parsed)
load_pWidth = nthelem(7 parsed)
load_pLength= nthelem(8 parsed)
tail_nWidth = nthelem(9 parsed)
tail_nLength= nthelem(10 parsed)
tail_pWidth = nthelem(11 parsed)
tail_pLength= nthelem(12 parsed)
VDD = nthelem(13 parsed)
;still need - (current Power GBW Load FOM)"
sprintf(path "/home/willyw/OceanSimdata/Inv_Opamp_char_8Multiple/%s" sim)
printf("sim - %s\n" path)
openResults(path)
selectResult("dcOp-dc")
Vout = v("voutn" ?result "dcOp-dc")
selectResult("dcOpInfo-info")
current = (pv("vSupply" "i" ?result "dcOpInfo-info")*-1)
Power = (pv("vSupply" "pwr" ?result "dcOpInfo-info")*-1)
Load = pv("C0" "cap" ?result "dcOpInfo-info")
selectResult("ac-ac")
GBW = unityGainFreq(v("voutn" ?result "ac-ac")/v("vinn" ?result "ac-ac"))
FOM = (pv("C0" "cap" ?result "dcOpInfo-info")*unityGainFreq(v("voutn" ?result "ac-
ac")/v("vinn" ?result "ac-ac"))*10E2)/(i("vSupply:p" ?result "dcOp-dc")*(-1))
; 1 2 3 4 5 6 7 8 9 10 11 12 13 14 15 16 17 18 19
```

```
sprintf(outstring "%s %s %s %s %s %s %s %s %s %s %s %g %g %s %g %g %g %g" in_nWidth
in_nLength in_pWidth in_pLength load_nWidth load_nLength load_pWidth load_pLength
tail_nWidth tail_nLength tail_pWidth tail_pLength current Vout VDD Power GBW Load FOM)
;printf("%s\n" outstring)
fprintf(p1 "%s\n" outstring)
)
close(p1)
```

Source code for data acquisition

```
function varargout = PlotVoltage(varargin)
% PLOTVOLTAGE M-file for PlotVoltage.fig
% PLOTVOLTAGE, by itself, creates a new PLOTVOLTAGE or raises the existing
% singleton*.
%
% H = PLOTVOLTAGE returns the handle to a new PLOTVOLTAGE or the handle to
% the existing singleton*.
%
% PLOTVOLTAGE('CALLBACK',hObject,eventData,handles,...) calls the local
% function named CALLBACK in PLOTVOLTAGE.M with the given input arguments.
%
% PLOTVOLTAGE('Property','Value',...) creates a new PLOTVOLTAGE or raises the
% existing singleton*. Starting from the left, property value pairs are
% applied to the GUI before PlotVoltage_OpeningFcn gets called. An
% unrecognized property name or invalid value makes property application
% stop. All inputs are passed to PlotVoltage_OpeningFcn via varargin.
%
% *See GUI Options on GUIDE's Tools menu. Choose "GUI allows only one
% instance to run (singleton)".
%
% See also: GUIDE, GUIDATA, GUIHANDLES
% Edit the above text to modify the response to help PlotVoltage
% Last Modified by GUIDE v2.5 15-Nov-2013 12:03:44
% Begin initialization code - DO NOT EDIT
gui_Singleton = 1;
gui_State = struct('gui_Name', mfilename, ...
'gui_Singleton', gui_Singleton, ...
'gui_OpeningFcn', @PlotVoltage_OpeningFcn, ...
'gui_OutputFcn', @PlotVoltage_OutputFcn, ...
```

```
'gui_LayoutFcn', [] , ...
'gui_Callback', []);
if nargin && ischar(varargin{1})
gui_State.gui_Callback = str2func(varargin{1});
end
if nargout
[varargout{1:nargout}] = gui_mainfcn(gui_State, varargin{:});
else
gui_mainfcn(gui_State, varargin{:});

end
% End initialization code - DO NOT EDIT
% --- Executes just before PlotVoltage is made visible.
function PlotVoltage_OpeningFcn(hObject, eventdata, handles, varargin)
% This function has no output args, see OutputFcn.
% hObject handle to figure
% eventdata reserved - to be defined in a future version of MATLAB
% handles structure with handles and user data (see GUIDATA)
% varargin command line arguments to PlotVoltage (see VARARGIN)
% Choose default command line output for PlotVoltage
handles.output = hObject;
% Initialize the "loopflag" field of the handles structure
handles.loopflag = false;
% Initialize the "haschannels" field of the handles structure
handles.haschannels = false;
% Initialize the "smooth100flag" field of the handles structure
handles.smoothpts = 0;
handles.ai_device0 = analoginput('mwadlink', 0);% Opens the analog input functionality
handles.ai_device1 = analoginput('mwadlink', 1);% Opens the analog input functionality
set(handles.ai_device0,'SampleRate', 10000);
set(handles.ai_device0,'SamplesPerTrigger', 100);
set(handles.ai_device0,'TriggerType', 'Immediate');
set(handles.ai_device0,'TriggerCondition', 'None');
set(handles.ai_device1,'SampleRate', 10000);
set(handles.ai_device1,'SamplesPerTrigger', 100);
set(handles.ai_device1,'TriggerType', 'Immediate');
set(handles.ai_device1,'TriggerCondition', 'None');
% Update handles structure
```

```
guidata(hObject, handles);
% UIWAIT makes PlotVoltage wait for user response (see UIRESUME)
% uiwait(handles.figure1);
% --- Outputs from this function are returned to the command line.
function varargout = PlotVoltage_OutputFcn(hObject, eventdata, handles)
% varargout cell array for returning output args (see VARARGOUT);
% hObject handle to figure
% eventdata reserved - to be defined in a future version of MATLAB
% handles structure with handles and user data (see GUIDATA)
% Get default command line output from handles structure

varargout{1} = handles.output;
% --- Executes on button press in start_pushbutton.
function start_pushbutton_Callback(hObject, eventdata, handles)
% hObject handle to start_pushbutton (see GCBO)
% eventdata reserved - to be defined in a future version of MATLAB
% handles structure with handles and user data (see GUIDATA)
% If we are already looping, exit early so that only one
% copy of the loop is executing
if handles.loopflag
return;
end
%if ~handles.haschannels
% return
%end
%plot(handles.axes1, xaxis, data);
count = 1;
% Set the flag, refresh the figure's GUIDATA to match "handles"
handles.loopflag = true;
guidata(hObject, handles);
data = [];
%cla(handles.axes1);
% On each loop check whether the flag has been reset
set(findall(handles.ChannelSelPanel, '-property', 'enable'), 'enable', 'off')
while handles.loopflag
start(handles.ai_device0);
wait(handles.ai_device0,30);
data = [data; getdata(handles.ai_device0)];
```

```
%data = [data; getsample(handles.ai_device0)];
%xaxis(count) = count;
%plot(xaxis,smooth(data,1000));
%plot(handles.axes1, x, y);
if handles.smoothpts == 0
plot(handles.axes1, data);
else
plot(handles.axes1, reshape(smooth(data,handles.smoothpts),size(data)));
end
%plot(handles.axes1, xaxis, data);
%set(handles.axes1, ...
%'YLim', [-2.5 2.5]);
count = count + 1;
%hist(smooth(data,1000),100);
drawnow;
% DRAWNOW both allows plotting events to execute, and gives a chance
% for other callbacks to interrupt
% This is in case the figure is killed ("X") while the loop is running
if ~ishandle(hObject)
return;
end
% Refresh "handles" to match the figure's GUIDATA
handles = guidata(hObject);
end
%scrollplot();
set(findall(handles.ChannelSelPanel, '-property', 'enable'), 'enable', 'on')
% --- Executes on button press in stop_pushbutton.
function stop_pushbutton_Callback(hObject, eventdata, handles)
% hObject handle to stop_pushbutton (see GCBO)
% eventdata reserved - to be defined in a future version of MATLAB
% handles structure with handles and user data (see GUIDATA)
% Set the flag, refresh the figure's GUIDATA to match "handles"
set(findall(handles.ChannelSelPanel, '-property', 'enable'), 'enable', 'on')
handles.loopflag = false;
guidata(hObject, handles);
% --- Executes on button press in radio10PtSmooth.
function radio10PtSmooth_Callback(hObject, eventdata, handles)
% hObject handle to radio10PtSmooth (see GCBO)
```

```
% eventdata reserved - to be defined in a future version of MATLAB
% handles structure with handles and user data (see GUIDATA)
% Hint: get(hObject,'Value') returns toggle state of radio10PtSmooth
handles.smoothpts = 10;
guidata(hObject, handles);
% --- Executes on button press in radio100PtSmooth.
function radio100PtSmooth_Callback(hObject, eventdata, handles)
% hObject handle to radio100PtSmooth (see GCBO)
% eventdata reserved - to be defined in a future version of MATLAB
% handles structure with handles and user data (see GUIDATA)
% Hint: get(hObject,'Value') returns toggle state of radio100PtSmooth
handles.smoothpts = 100;
guidata(hObject, handles);
% --- Executes on button press in radio1000PtSmooth.
function radio1000PtSmooth_Callback(hObject, eventdata, handles)
% hObject handle to radio1000PtSmooth (see GCBO)
% eventdata reserved - to be defined in a future version of MATLAB
% handles structure with handles and user data (see GUIDATA)
% Hint: get(hObject,'Value') returns toggle state of radio1000PtSmooth
handles.smoothpts = 1000;
guidata(hObject, handles);
% --- Executes on button press in radioSmooth0Pt.
function radioSmooth0Pt_Callback(hObject, eventdata, handles)
% hObject handle to radioSmooth0Pt (see GCBO)
% eventdata reserved - to be defined in a future version of MATLAB
% handles structure with handles and user data (see GUIDATA)
% Hint: get(hObject,'Value') returns toggle state of radioSmooth0Pt
handles.smoothpts = 0;
guidata(hObject, handles);
% --- Executes on button press in TestAqButton.
function TestAqButton_Callback(hObject, eventdata, handles)
% hObject handle to TestAqButton (see GCBO)
% eventdata reserved - to be defined in a future version of MATLAB
% handles structure with handles and user data (see GUIDATA)
%%getsample(handles.ai_device)
handles.ai_device0
handles.ai_device1
```

```
%%%%%%%%%%%%%%%%%%%%%%%%%%%%%%%%%%%%%%%%%%%%%%%%%%%%%%%%%
%%
% Channel Box Callbacks
%%%%%%%%%%%%%%%%%%%%%%%%%%%%%%%%%%%%%%%%%%%%%%%%%%%%%%%%%
%%
% --- Executes on button press in Ch1chkbox.
function Ch1_0chkbox_Callback(hObject, eventdata, handles)
% hObject handle to Ch1chkbox (see GCBO)
% eventdata reserved - to be defined in a future version of MATLAB
% handles structure with handles and user data (see GUIDATA)
% Hint: get(hObject,'Value') returns toggle state of Ch1chkbox
%if ~handles.haschannels
% handles.haschannels = true;
%end
if get(hObject,'Value') %if box is NOT checked
handles.ai0_1 = addchannel(handles.ai_device0, 1);%Add channel #0 to ai_device
set(handles.ai0_1, 'InputRange', [-2.5 2.5]);
else %box is checked
end
% --- Executes on button press in Ch2_0chkbox.
function Ch2_0chkbox_Callback(hObject, eventdata, handles)
% hObject handle to Ch2_0chkbox (see GCBO)
% eventdata reserved - to be defined in a future version of MATLAB
% handles structure with handles and user data (see GUIDATA)
% Hint: get(hObject,'Value') returns toggle state of Ch2_0chkbox
if get(hObject,'Value') %if box is NOT checked
handles.ai0_2 = addchannel(handles.ai_device0, 2);%Add channel #0 to ai_device
set(handles.ai0_2, 'InputRange', [-2.5 2.5]);
else
end
```

Biography

Project Leader

Name	Weerachon Phoohinkong
Work Position	Researcher, Faculty of Science And Technology, Suan Dusit University
Educational Attainment	M.Sc.(Chemistry), KMITL B.Sc. (Chemistry), Kasetsart University
Research Interests	Electronics, Nanomaterial, Analytical Chemistry, Electrochemistry, Biosensors

Researcher 1

Name	Yutthana Phimthong-Ngam
Work Position	Instructor, Physics Education Program, Faculty of Science and Technology, Suan Dusit University
Educational Attainment	Ph.D. (Medical Engineering), Thammasat University M.Sc.(Materials Science), Chulalongkorn University B.Sc. (Physics), Kasetsart University
Research Interests	Physiological Modeling and Simulation, Bioinformatics, Pattern Recognition, Artificial Intelligence, Medical Sensors and Signal Processing, Embedded Systems

Researcher 2

Name	Rattapong Sungnoon
Work Position	Physician, Department of Physiology Faculty of Medicine Chiang Mai University
Educational Attainment	Ph.D. (Medical Engineering), Thammasat University M.D. (Medicine), Chiang Mai University
Research Interests	Cardiovascular Physiology and Cardiac Electrophysiology

Researcher 3

Name	Harutai Khunphet
Work Position	Public Health Laboratory, Ban Poeng Kheling Health Center, Umphang, Tak
Educational Attainment	B.P.H. (Public health), Naresuan University
Research Interests	Public Health

Researcher 4

Name	Laddawan Sangsoda
Work Position	Public Health Laboratory, Khok Samran Health Center, Ban Kluai, Chon Daen, Phetchabun
Educational Attainment	B.P.H. (Public health), Naresuan University
Research Interests	Public Health

Researcher 5

Name	Kanyanat Kongnonglan
Work Position	Public Health Laboratory, Somdet Phra Yuppharat Hospital , Nakhon Thai, Phitsanulok
Educational Attainment	B.P.H. (Public health), Naresuan University
Research Interests	Public Health